Journal of Research of the National Bureau of Standards Vol. 60, No. 3, March 1958 Research Paper 2843

Fragmentation of Waterdrops in the Zone Behind an Air Shock*

Olive G. Engel

Observations made on the fragmentation of two waterdrop sizes, after collision with air shocks that were moving at three different supersonic velocities, are reported. The possible mechanisms of various aspects of the fragmentation process are discussed. The experimental observations indicate that high-speed-rain-erosion damage should not be observed on spheres having a diameter as large as 4 feet and moving with a Mach number in the range of 1.3 to 1.7 in rain that has a drop diameter of 1.4 millimeter. Waterdrops of this size should be reduced to mist in the zone of separation between the detached shock and the surface of the sphere according to the results that are reported. A means to extend this protection to spheres of smaller diameter or to rain of larger size is pointed out. The need for further experimental observation of the time required for the fragmentation of waterdrops using shocks moving at higher Mach numbers is indicated to verify and extend the information.

1. Introduction

A blunt object moving through air at supersonic velocity is preceded by a detached shock wave that is separated from the leading surface of the object by a zone in which air is moving forward at high velocity in front of the object. It has been shown [1] that if a waterdrop were subjected to the conditions that prevail in the zone of detachment between such a shock wave and the object (Mach number 1.7) that is producing it, the waterdrop would be reduced to droplets having diameters of the order of millionths of a foot. Droplets of this size are probably incapable of causing erosion of the surface of the object when they are intercepted by it, even though the object is moving at supersonic velocity. This follows because small drops are so much less effective than large drops in producing waterdrop impingement damage. If, therefore, the waterdrop has time to fragment into droplets before the surface of the object that is producing the shock intercepts it, the problem of erosion as a result of high-speed-rain impingement may be less serious at supersonic velocities than at subsonic velocities. A study of the breakup of waterdrops in high velocity airflows produced by a blast gun has been made at Porton in England. However, published reports of this work do not contain the quantitative information that is needed. To obtain this information, the photographic observation of the fragmentation of waterdrops in a shock tube was undertaken.

It was conjectured that the time required for the fragmentation of liquid drops under the conditions that exist behind an air shock would be found to be a function of several variables. For drops of distilled water these variables should reduce to the velocity of the air shock and the mass of the drop. Therefore, data were collected over a range of three air-shock velocities (Mach number of the shock was 1.3, 1.5, and 1.7) for both a large (2.7-mm diam) and a small (1.4-mm diam) drop size, respectively.

Results of this investigation indicate that high-speed-rain-erosion damage should not be observed on spheres having a diameter as large as 4 ft and moving with a Mach number in the range of 1.3 to 1.7 in rain that has a drop diameter of 1.4 mm. See section 5. Drops of this size should be reduced to mist in the zone of separation between the detached shock and the surface of the sphere according to the observations that have been made. It may be possible by means of design to extend this protection to spheres of smaller diameter or to rain of larger drop size. See section 5.

2. Details of the Observation Arrangement

Observations of the type required can be made best in a shock tube in which the velocity of the air shock can be controlled within a small range of variation and through which permanent photographic recording is possible. In order to take spark pictures of the waterdrop at known time intervals after it is struck by an air shock, a shock tube containing large planar glass windows is required.

2.1. Description of the Shock Tube and Waterdrop Source

The shock tube used was located at the Naval Ordnance Laboratory at White Oak, Maryland. It has been described previously [1].[2] The 4-ft pressure chamber of this tube was separated from the 14-ft expansion chamber by a plastic film. See figure 1. The pressure chamber was filled with helium gas to a gage pressure that was found sufficient to produce the required air-shock velocity. Sudden release of this gas by puncturing the plastic film with a needle plunger resulted in the formation of an air shock in the column of air that occupied the expansion chamber.

The exit end of the expansion chamber contained 3- by 8-in. glass windows of interferometric quality. To admit waterdrops, a set of ½-in.-diam holes was bored through the top and bottom walls of the shock tube at the left-hand side of the window. A fiducial marker was used to indicate the centers of these holes. An additional set of holes existed at the center of the window.

Drops of distilled water were formed at the tip of a hypodermic needle that was mounted above the

[1] Unpublished data of the author.

*The work described in this paper was sponsored by the Wright Air Development Center whose assistance and interest are gratefully acknowledged.

[2] Figures in brackets indicate the literature references at the end of this paper.

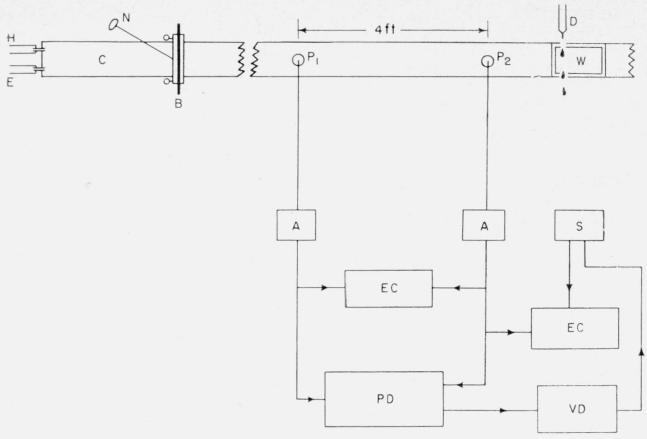

FIGURE 1. *Shock tube and electronic circuits.*

A, amplifier; B, plastic film barrier; C, high pressure chamber; D, waterdrop source; E, exhaust; EC, electronic counter; H, helium intake; N, needle plunger to puncture barrier; P_1, P_2, pressure pickups; PD, proportional delay; S, spark; VD, variable delay unit; W, glass window.

shock tube. The drops were allowed to fall through the holes in the tube into a reservoir located below the underside of it. The freely falling waterdrops were photographed at various time intervals after they were intercepted by an air shock. With use of this arrangement, every spark picture that was taken was of a different waterdrop. Due to the way in which the waterdrop fell from the needle and to adjustments of the needle itself, the waterdrops did not always fall on exactly the same path through the holes in the shock tube. This resulted in a certain amount of horizontal scatter in the location of the waterdrop at the time that the air shock collided with it. This horizontal scatter in the fall trajectories of the drops proved to be a disadvantage both in calculating the time that elapsed from the air-shock-waterdrop collision to the taking of the picture and in determining the drift of the waterdrop in the airstream behind the shock during the time interval from the collision instant to the instant that the picture was made. The scatter was greater in the case of small waterdrops, which were formed at the tip of a hypodermic needle of small bore, than in the case of large waterdrops, which were formed at the tip of a hypodermic needle of large bore.

The sizes of the drops that were produced varied with the rate at which the drops were formed at the tip of the hypodermic needle. When the dropping rate was such as to place only one drop in the picture with use of the small-bore needle, the drop was nearly as large as those formed at the same rate by the large-bore needle. It was, therefore, necessary to have more than one drop in the picture in the case of the small drops in order to have a notable difference in drop size to observe the effect of water mass on the time required for waterdrop fragmentation.

2.2. Photographic Recording

The shock tube extended from the NOL Ballistics Range Laboratory into a small adjoining room which served as the camera box as well as for a photographic dark room. The pressure chamber and the major part of the expansion chamber of the shock tube were in the main laboratory; the exit end, which contained the glass windows through which the photographic observations were made, was housed in the auxiliary room.

The light source for the pictures was a 1-μsec spark. See figure 2. Light from the spark was collimated and the collimated beam was passed through the windows of the shock tube. It was then concentrated by the field lens and focused by the camera lens on film that was exposed in darkness in the auxiliary room just before a picture was made. The spark appears as a dim circle of light in the pictures.

Pictures taken in this optical system were all originally about 1.4 $\times$. Figures 7 and 9 are enlargements of original photographs.

2.3. Time Measurement

The velocity at which the air shock was moving down the shock tube was calculated from the time that was required for it to traverse a known distance between two points. Two barium titanate pressure pickups were inserted 4 ft apart in the wall of the shock tube. See figure 1. Signals received by these pressure pickups, when the air shock passed them in its progress down the tube, were used to start and to stop a Potter electronic counter. The reading on this counter was the time in microseconds required for the air shock to move the 4-ft distance between the pressure pickups.

The time that elapsed between the instant that the air shock intercepted the waterdrop and the instant that the picture was made was found by measuring the distance between the air shock and the center of the waterdrop as seen in the picture itself. Eventually, a time was reached at which the air shock had progressed beyond the right-hand boundary of the picture. For the time range in which no shock was visible in the picture, a second Potter electronic counter was used to determine the time that had elapsed between the air-shock-

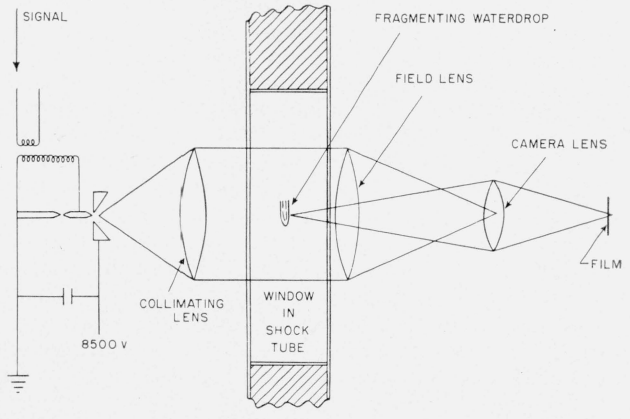

FIGURE 2. *Optical arrangement and spark.*

waterdrop collision and the instant that the picture was taken. This counter was started by the signal from the second pressure pickup and was stopped at the instant that the spark for the picture was set off. The time that elapsed from the instant that the shock passed the fiducial marker to the instant that the spark for the picture went off was found by subtracting the observed time required for the shock to advance from the second pressure pickup to the fiducial marker from the second counter reading.

2.4. Conditions in the Airflow Behind a Shock That Moves Into Still Air

The conditions that exist in the air through which the shock has moved constitute the environment in which the waterdrop finds itself after the air-shock-waterdrop collision.

a. Velocity of the Airstream That Exists Behind a Moving Shock

The velocity of the airstream in which the waterdrop finds itself after the air shock has intercepted it and passed by is an important factor in the fragmentation of the waterdrop. For the case of a stationary shock formed in a shock tube, the continuity equation is

$$\rho_1 u_1 = \rho_2 u_2 \tag{1}$$

so that

$$u_2 = \frac{\rho_1}{\rho_2} u_1 \tag{2}$$

where u_1 is the velocity of the airstream entering the shock and ρ_1 is the density of this air, u_2 is the velocity of the airstream after passing through the shock, and ρ_2 is the density of this air.

For the case of a moving shock, the airstream velocities on either side of the shock are those seen by an observer who is moving toward the shock at the velocity u_1. For this observer the velocity of air approaching the shock is U_1 and

$$U_1 = 0. \tag{3}$$

The shock appears to be approaching this observer at a velocity U_s, and

$$U_s = -u_1. \tag{4}$$

The velocity of air on the opposite side of the shock as seen by this observer is U_2 and

$$U_2 = u_2 - u_1 \tag{5}$$

or, by use of eq (2),

$$U_2 = \left[\frac{\rho_1}{\rho_2} - 1\right] u_1. \tag{6}$$

In terms of the velocity of the shock, by use of eq (4),

$$U_2 = U_s \left[1 - \frac{\rho_1}{\rho_2}\right] \tag{7}$$

from which it can be seen that U_2 is constant for any given shock velocity. For the moving air shock, the sub-1 notation applies to the undisturbed air ahead of the shock and the sub-2 notation applies to the air through which the shock has passed. In terms of the Mach number of the shock, M_s, the inverse of the air density ratio is [2]

$$\rho_2/\rho_1 = (\gamma+1)M_s^2/[(\gamma-1)M_s^2+2]. \tag{8}$$

The constant velocity of the air behind a shock moving down a shock tube can be calculated, therefore, if only the velocity of the shock itself is known. The velocity of the airstream behind the shock can also be calculated from the expression given in reference [3]

$$U_2 = (U_s^2 - c_1^2)/2U_s[(\gamma+1)/4] \tag{9}$$

where c_1 is the speed of sound in the undisturbed air ahead of the moving shock and γ is the ratio of the specific heat at constant pressure to the specific heat at constant volume, which for air is 1.4.

The calculated values of the velocity of the airflow behind shocks that have Mach numbers of 1.3, 1.5, and 1.7 are given in table 1.

b. Temperature of the Air Behind the Moving Shock

A knowledge of the temperature of the air in which the fragmentation of a waterdrop occurs is of interest in establishing the mechanism of the fragmentation process. The ratio of the temperature of the airstream behind the moving shock, T_2, to the temperature of the undisturbed air into which the shock is advancing, T_1, is given by the expression [2]

$$T_2/T_1 = [2\gamma M_s^2 - (\gamma-1)][(\gamma-1)M_s^2+2]/(\gamma+1)^2 M_s^2. \tag{10}$$

TABLE 1. *Conditions in the constant-velocity airstream flowing behind the air shock*

Shock, Mach number, M_s	Conditions in the constant-velocity airstream flowing behind the air shock (assuming that ρ_1=0.0011766 g/cm³; T_1=300° K; μ_1=184.2 micropoise)										
	Velocity, U_2	Sound speed, c_2	Mach number, M_2	Density, ρ_2	Temperature, T_2		Pressure, p_2	Stagnation pressure, p_t	Viscosity, μ_2	Kinematic viscosity, μ_2	Reynolds number for the 2.7-mm-diameter waterdrop
	cm/sec	*cm/sec*		*g/cm³*	*° K*	*° C*	*Dynes/cm²*	*Dynes/cm²*	*Poise*	*cm²/sec*	
1.3	1.52×10⁴	3.75×10⁴	0.4	0.00178	357	84	1.79×10⁶	1.99×10⁶	2.10×10⁻⁴	0.118	35,000
1.5	2.37	3.96	.6	.00218	396	123	2.43	3.10	2.27	.104	61,000
1.7	3.16	4.16	.76	.00256	438	165	3.17	4.65	2.46	.096	89,000

The calculated values of the temperature of the air that is flowing behind shocks that have Mach numbers of 1.3, 1.5, and 1.7, taking the temperature of the undisturbed air ahead of the advancing shock to be 300° K, are given in table 1.

c. Viscosity of the Air Behind the Moving Shock

It is necessary to know the viscosity of the air that is flowing behind the moving shock to evaluate the Reynolds number of the airflow around the waterdrop. The viscosity coefficient of the air flowing behind the shock, μ_2, can be approximated from the expression [2]

$$\mu_2/\mu_1=(T_2/T_1)^{0.76}. \tag{11}$$

The calculated values of the viscosity coefficient of the air flowing behind shocks having Mach numbers of 1.3, 1.5, and 1.7, found by use of eq (10) and by taking the viscosity of the undisturbed air ahead of the advancing shock to be 184.2 μpoise, are given in table 1. The calculated values of the density, ρ_2, and of the kinematic viscosity, ν_2, of the air flowing behind shocks having these Mach numbers, found by use of eq (8) and by taking the density of the undisturbed air ahead of the advancing shock to be 0.0011766 g/cm^3, are also given in table 1.

d. Reynolds Number for the Flow Around the 2.7-mm Diameter Waterdrop

Knowing the velocity, U_2, the viscosity coefficient, μ_2, and the density, ρ_2, of the airstream that is flowing behind the shock, the Reynolds number of the flow around the waterdrop, $\rho_2 U_2 l/\mu_2$, where l is a characteristic length, can be calculated. The drift velocity has been neglected. The values of the Reynolds number of the flow around the 2.7-mm-diam waterdrop, taking l to be the diameter of the drop, are given in table 1 for the case that the Mach number of the shock was 1.3, 1.5, and 1.7.

e. Mach Number of the Airstream Flowing Behind the Moving Shock

To determine the Mach number of the airflow behind the moving shock, M_2, it is necessary to know the speed of sound in this air, c_2. The sound speed can be calculated from the expression given in [3]

$$c_2^2=c_1^2+\frac{2(\gamma-1)}{(\gamma+1)^2}\left[\gamma U_s^2-(\gamma-1)c_1^2-\frac{c_1^4}{U_s^2}\right] \tag{12}$$

where c_1 is the speed of sound in the undisturbed air ahead of the shock. The values of the sound speed and of the Mach number of the airflow behind the shock, U_2/c_2, found by use of eq (7) and (12) are given in table 1 for the condition that the Mach number of the shock is 1.3, 1.5, and 1.7.

f. Pressure in the Airstream Flowing Behind the Moving Shock

A knowledge of the free-stream pressure in the airflow behind the moving shock is needed to determine the pressure that exists on the windward and leeward faces of the waterdrop. The free-stream pressure, p_2, is given by [3]

$$p_2=p_1+\rho_1 U_s U_2, \tag{13}$$

and because

$$p_1=c_1^2\rho_1/\gamma, \tag{14}$$

$$p_2=\rho_1\left[\frac{c_1^2}{\gamma}+U_2U_s\right]. \tag{15}$$

Taking ρ_1 to be 0.0011766 g/cm^3, c_1 to be 3.44x10^4 cm/sec, and using the values of U_2 found from eq (7), the values of p_2 were found for the condition that the Mach number of the shock was 1.3, 1.5, and 1.7. They are listed in table 1.

2.5. Pressure on the Windward and Leeward Faces of a Waterdrop in an Airstream

As soon as an air shock intercepts a waterdrop, the waterdrop exists in the airstream behind the shock, and pressure differences are established around it. Potential flow, in which there are no vortices, exists at first. There is a high pressure at the stagnation point in the center of both the windward and leeward face of the waterdrop, and these pressures are equivalent as long as potential flow persists. Low pressure exists at the equatorial belt between the two stagnation points. Eventually vortices appear at the leeward face of the drop. The pressure at the leeward face of the drop then falls to a value that is only slightly higher than that at the equatorial belt.

Fage [4] measured the pressure that developed on a 6-in.-diam sphere in an airflow. For Reynolds numbers up to 424,500, the results of Fage indicate that the pressure distribution on the windward face is essentially unchanged as the Reynolds number is increased but that at high Reynolds numbers the pressure drop around the equatorial belt becomes more intense and the pressure on the leeward face rises. Comparison of the values obtained for Reynolds number of 110,000 and 157,200 shows that there is little difference in them except that the pressure drop around the equatorial belt is less for the lower Reynolds number. In view of the value of the Reynolds number for the flow around the 2.7-mm-diam waterdrop when it exists in the airstream behind shocks having Mach numbers of 1.3, 1.5, and 1.7 (see table 1), it can be expected that the pressure distribution around it is closely the same as that found by Fage for a Reynolds number of 110,000 except that the minimum in the curve at an angle of about 75° is probably less pronounced. See section 4.7.

a. Stagnation Pressure on the Windward Face of the Waterdrop

The highest pressure that is developed on a waterdrop, which exists in the airflow behind an air shock, occurs at the center of the windward face. This is the stagnation point where the airstream velocity is zero. If the air is brought to rest isentropically, the

stagnation pressure is given by the expression [2]

$$p_2/p_t=\left[1+\frac{(\gamma-1)}{2}M_2^2\right]^{-\gamma/(\gamma-1)} \quad (16)$$

where p_t is the total pressure at the stagnation point. Values of p_t, which were calculated with use of values of p_2 obtained from eq(15) and with use of values of M_2 obtained from eq (7) and (12) for the condition that the Mach number of the shock is 1.3, 1.5, and 1.7, are given in table 1.

b. Pressure on the Leeward Face of the Waterdrop

After vortices form at the leeward face of the waterdrop, the pressure there drops to a value below the stagnation-point pressure on the windward face of the drop. From the data of Fage [4],

$$p_L-p_2=-0.4(\tfrac{1}{2}\rho_2 U_2^2) \quad (17)$$

where p_L is the leeward face pressure. Because

$$\rho_2=\gamma p_2/c_2^2, \quad (18)$$

$$p_L=p_2[1-(0.2\gamma U_2^2/c_2^2)]. \quad (19)$$

Using eq (9), (12), and (15), the value of p_L for a waterdrop that exists in the airflow behind a shock having a Mach number of 1.3 is 1.71×10^6 d/cm^2 (1.69 atm).

2.6. Temperature on the Windward and on the Leeward Face of a Waterdrop in an Airstream

If the airstream is brought to rest isentropically, the stagnation-point temperature, T_t, at the center of the windward face is given by the expression [2]

$$T_2/T_t=\left[1+\frac{(\gamma-1)}{2}M_2^2\right]^{-1}. \quad (20)$$

When the Mach number of the air shock is 1.3, T_t is found to be 368°K (95°C) by use of eq (7), (10), and (12).

It is necessary to know the air density at the leeward face of the drop to evaluate the leeward-face temperature. From the adiabatic equations

$$p_2=(\text{constant})\rho_2^{\gamma}, \quad (21)$$

$$p_L=(\text{constant})\rho_L^{\gamma}, \quad (22)$$

it follows that

$$\rho_L=\rho_2\sqrt[\gamma]{\frac{p_L}{p_2}}. \quad (23)$$

When the Mach number of the air shock is 1.3, ρ_2 is 0.00178 g/cm^3 (see section 2.4.c). From eq (23), ρ_L is then 0.00172 g/cm^3. Because

$$p_L=\rho_L R T_L$$

$$T_L=p_L/R\rho_L. \quad (24)$$

Using the value of p_L found in section 2.5.b, the value of the gas constant, R, in ergs per degree per gram, and the value of ρ_L found just above, T_L is 353° K (80° C) when the Mach number of the shock is 1.3.

3. Observed Stages in the Fragmentation of Two Waterdrop Sizes After Collision with Air Shocks that Were Moving at Three Different Velocities

The dropping rates used were such that waterdrops formed with use of the large hypodermic needle had an approximate average diameter of 2.7 mm and waterdrops formed with use of the small hypodermic needle had an approximate average diameter of 1.4 mm.

3.1. Mach Number of the Shock Is 1.3

The observed stages in the fragmentation of the large and of the small waterdrop in the airflow behind the shock when the Mach number of the shock was 1.3 are given in the following two sections. The velocity of the airflow behind the shock, which is the environment in which the fragmentation is accomplished, is 1.52×10^4 cm/sec for this air-shock velocity.

a. Stages in the Fragmentation of the Large Waterdrop

Casual inspection of a spark picture taken of a 2.7-mm-diam waterdrop 76 μsec after it was struck by an air shock leaves the impression that it is undisturbed. Actually, this is not the case. The high light in the shadowgraph of the drop, which appears as a dim pinpoint of light to the unaided eye, has a distinct structure at low magnification. It consists of a starlike cluster of sharp prongs of light. This is quite different from the appearance of the high light in a waterdrop that has not been struck by an air shock. In the undisturbed drop the high light is more or less circular and has little structure. More is said about this observation in section 3.2.a, and the possible significance of it is discussed in section 4.2. In a picture taken 84 μsec after the air-shock-waterdrop collision, the high light in the drop was so dim that the exact structure of it could not be determined. In addition to the change in the appearance of the high light, there is a slight corrugation on the windward face of the drop. The corrugation of the windward face is also evidence that the drop is not quiescent.

The first response of a waterdrop of this size that can be detected with the unaided eye is apparent in a spark picture taken at the end of 93 μsec after the air-shock-waterdrop collision. See figure 3, picture 1. The leeward face of the waterdrop appears to be flattened in this picture, and there is some evidence of the start of a radial flow of water from the drop in a plane through the center of it that is also perpendicular to the wind direction. This is manifested by a slightly pointed appearance of the top and bottom of the drop as it is viewed in the picture. The points are somewhat more apparent on the waterdrop

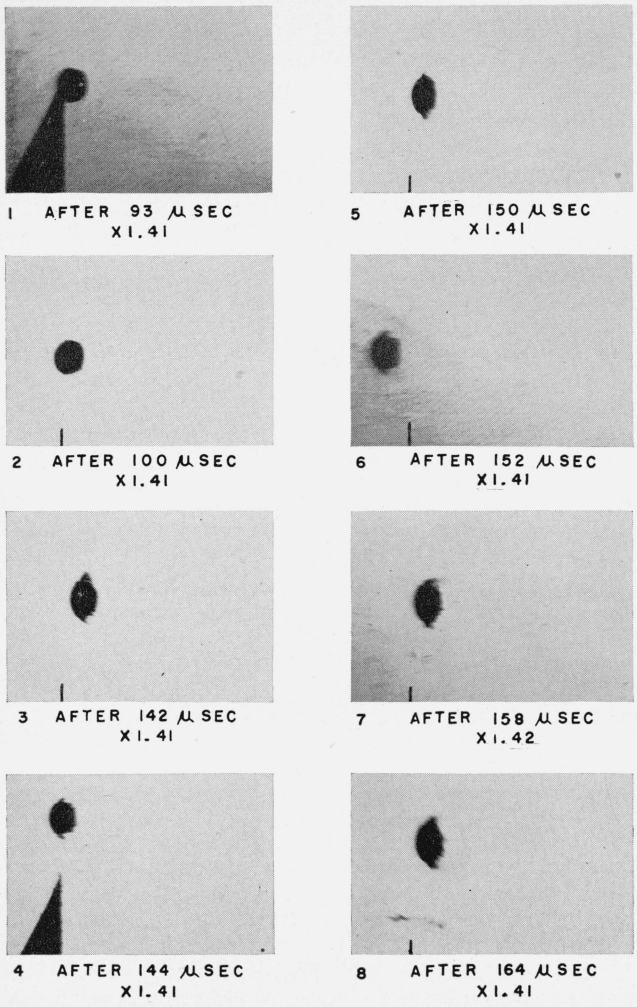

FIGURE 3. *Views of the 2.7-mm-diam waterdrop showing the flattening of the leeward face (right-hand side) of the drop, the development of the radial flow, the beginning of the formation of water mist, and the flattening of the drop perpendicular to the wind direction.*

Mach number of the air shock was 1.3.

shown in figure 3, picture 2, which was taken 100 μsec after the air-shock-waterdrop collision. The flattening of the leeward face of the waterdrop is discussed in section 4.3. The radial flow of the drop becomes more marked with the passage of time after the air-shock-waterdrop collision; the length of the protrusions increases with the time elapsed since the collision incident. The flow is, of course, not two spouts of water from the top and bottom of the drop as it is observed in the pictures; it is a ring of water moving radially out of the drop and appears as the rings of Saturn do when they are viewed on edge. From the pictures of figure 3 it can be seen that after this ring of water has moved out far enough from the drop, it is bent in the wind direction (toward the right) by the force of the rapid airflow. Possible causes of this radial flow of water from the drop are discussed in section 4.5.

The radial flow is accompanied by another process that is more important as far as the fragmentation of the waterdrop is concerned. This is the formation of water mist. Evidence of the formation of mist from the radially flowing water and from the leeward face of the waterdrop can be seen in figure 3, pictures 3 through 8. The limiting stage to which the mist formation goes can be seen in figure 4. In figure 4, picture 6, the streamers of mist extend to the right-hand boundary of the picture. Mechanisms that may be responsible for the formation of this mist are discussed in section 4.4.

The formation of water mist and of the beginning of radial water flow are accompanied by a gradual flattening of the drop, that is, by an increase in its diameter in all directions perpendicular to that of the rapid airflow. A graph of the measured values of the maximum diameter of 2.7-mm-diam waterdrops, after various intervals of time up to 420 μsec after they were struck by an air shock, is shown in figure 5. There are four distinct regions in the curve. The first region is a plateau from zero time after the air-shock-waterdrop collision to about 90 μsec after the collision incident. This corresponds with the time during which the waterdrop appears to be quiescent. Inspection of the experimental curves for the flattening with time after 2.7-mm-diam waterdrops collided with shocks when the Mach number of the shock was 1.5 and 1.7 (see fig. 5) leads to the conclusion that a very slight flattening probably does occur during at least part of the period of apparent quiescence and/or that the length of the period of quiescence is a function of the Mach number of the shock.

The second region in the curve of waterdrop flattening, as a result of collision with air shocks when the Mach number of the shock was 1.3, is an almost linear increase of the drop diameter perpendicular to the direction of the airflow. That the flattening is not a linear function of the time but that instead there is a very slight increase in the degree of flattening with time, can best be seen by inspection of the flattening curves when the Mach number of the air shock was 1.5 and 1.7. For the case of air-shock-waterdrop collisions when the Mach number of the shock was 1.3, the flattening appears to terminate at the end of 220 μsec after the collision incident.

The third region in the curve extends from 220 μsec to about 300 μsec. It is a plateau and the existence of it appears to indicate that at the end of 220 μsec the water of the drop has given a maximum response to the pressure difference that is set up by the airflow between the poles and the equator of it. Further flattening appears to be checked. Because a similar plateau appears to exist in the flattening curve at about this same time interval for the case that the Mach number of the shock was 1.5, it seems likely that it is the force of surface tension that acts as a check against further flattening of the drop. See section 4.6 and, for a further discussion of this point, section 4.8.

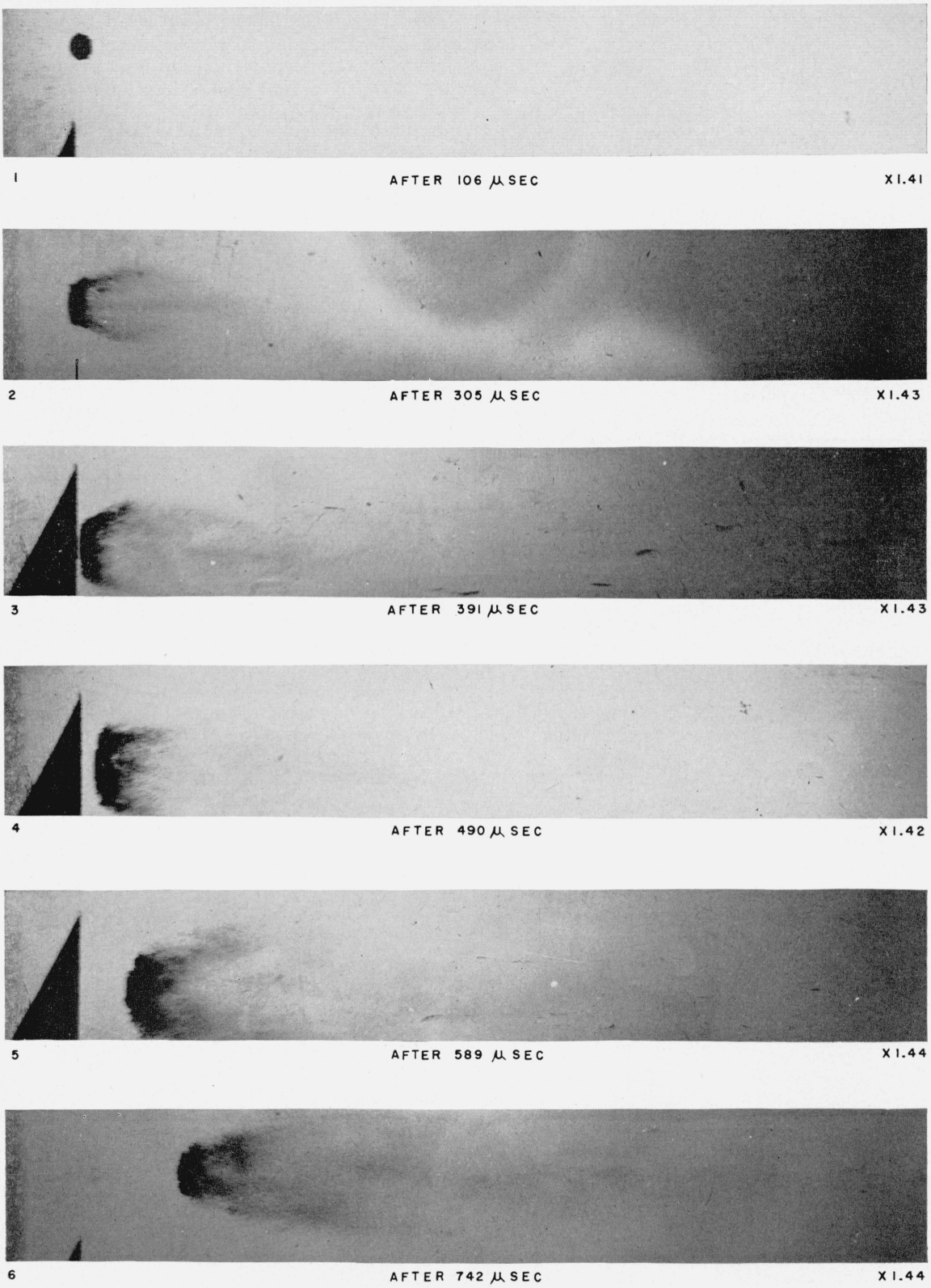

FIGURE 4. *Stages in the fragmentation of a 2.7-mm-diam waterdrop.*

Mach number of the air shock was 1.3.

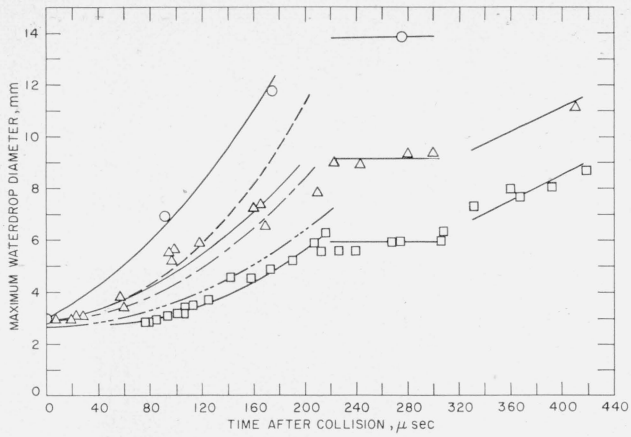

FIGURE 5. *Flattening of waterdrops after collision with air shocks having Mach numbers of 1.3, 1.5, and 1.7.*

Mach number of shock	
Empirical curve	Calculated curve
○, 1.7	— — —, 1.7
△, 1.5	— - —, 1.5
□, 1.3	— - - - —, 1.3

In the fourth region, the diameter of the drop perpendicular to the direction of the airflow down the shock tube again increases, but the increase is at a slower rate. The intact portion of the waterdrop eventually segments. The fourth region of the flattening curve of figure 5 may mark the drifting apart of the separate segments of the waterdrop after segmentation has occurred.

It might be supposed that the waterdrop would start to move down the shock tube with the airstream as soon as the air shock had struck it and passed by. This, however, does not seem to be the case. Measurements of the distance from the edge of the fiducial marker to the leading edge of the waterdrop at various time intervals after a 2.7-mm-diam waterdrop collided with an air shock when the Mach number of the shock was 1.3 indicate that there was essentially no drift under 100 μsec after the collision incident. These data are not presented, but the condition of essentially no drift in the initial 100 μsec after the air-shock-waterdrop collision can be seen in graphs of similar data for collision of 2.7-mm-diam waterdrops with air shocks when the Mach number of the shock was 1.5 and 1.7. See figure 6, A and 6, B. The drift velocity of the waterdrop is discussed in section 4.7.

The final stages of the disintegration of the waterdrop are a distinct corrugation of its windward face followed by breakup of the remaining portion of the waterdrop into separate sections. From a comparison of calculated with observed values of the acceleration of the waterdrop in the airflow behind a shock, it appears likely that a hole forms in the disk of water to which the waterdrop flattens. See section 4.7. If, indeed, a hole is forced through the water disk in the early stages of the fragmentation process, the final stage is a segmentation of the resulting water ring into a chain of water beads.

b. Stages in the Fragmentation of the Small Waterdrop

The large waterdrop shows essentially no response 76 μsec after the passage of the air shock. The small waterdrops are streaming water mist and are in an advanced stage of radial flow 75 μsec after the passage of the shock. At the end of 93 μsec after

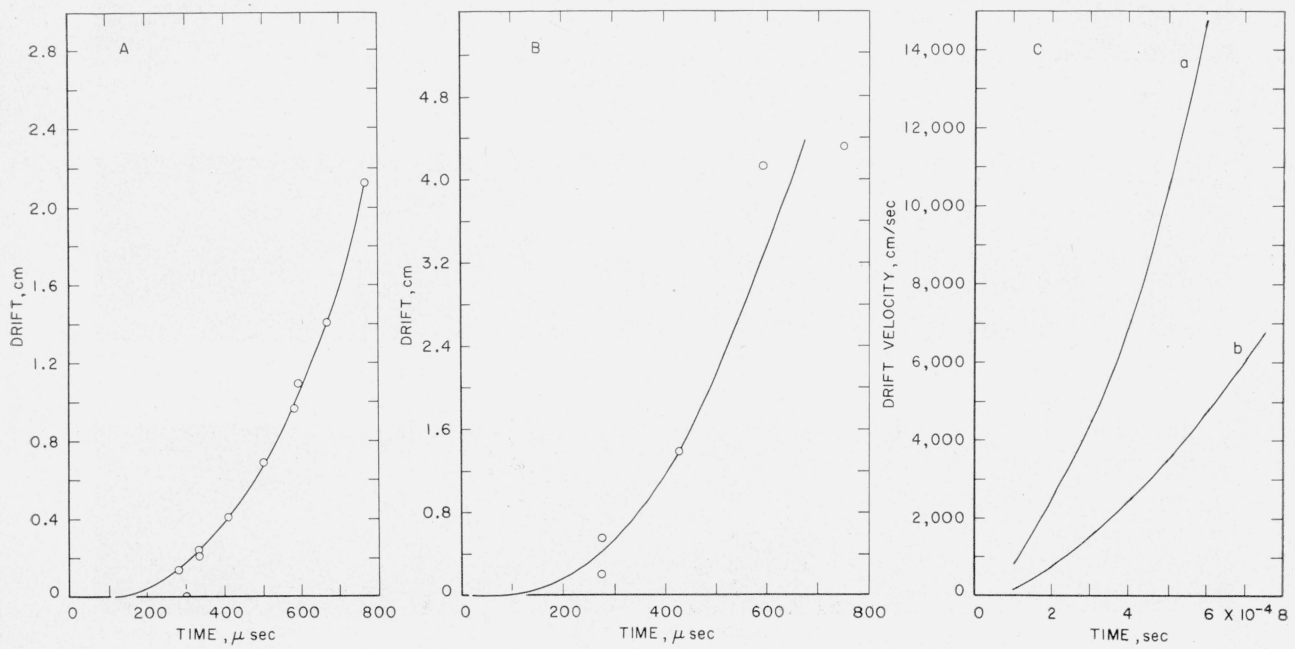

FIGURE 6. *A, Drift of 2.7-mm-diam waterdrops after collision with air shocks that had a Mach number of 1.5; B, drift of 2.7-mm-diam waterdrops after collision with air shocks that had a Mach number of 1.7; C, plot of drift velocity versus time for 2.7-mm-diam waterdrops.*

a) Mach number of the air shock was 1.7, and (b) Mach number of the air shock was 1.5.

the collision, the large waterdrop has only responded to the extent of developing a square appearance of the leeward face. By the end of less time than this, that is, after 82 and after 88 μsec, the small drops have flowed radially and have flattened in a plane perpendicular to the direction of motion of the shock and are emitting water mist both from the leeward face and from the periphery of the radial flow. A comparable stage of fragmentation is reached for the large waterdrop only at the end of about 200 μsec after the air-shock-waterdrop collision. From these observations, the large waterdrop is lagging the small waterdrop by better than 100 μsec in developing an initial stage of fragmentation.

Evidence of the corrugation of the windward face of the small waterdrop can be seen at the end of 75 μsec after the air-shock-waterdrop collision, and strong corrugation of the windward face can be seen 160 and 170 μsec after the collision incident. The stage of fragmentation reached by the small waterdrops 230 μsec after the air-shock-waterdrop collision about compares with that reached by the large waterdrop at the end of 331 μsec. In the development of this stage of fragmentation, the large waterdrop has again lagged behind the small waterdrop by about 100 μsec.

At the end of 593 μsec after the air shock collided with the waterdrop, the remaining portion of the small waterdrop is seriously corrugated; 698 μsec after the collision incident, the remaining portion of the small waterdrop is broken up. The remaining segments of the drop continue to emit water mist. The breakup of the intact portion of the large waterdrop when the Mach number of the shock was 1.3 was not observed; it occurs at a time longer than 742 μsec after the air-shock-waterdrop collision.

3.2. Mach Number of the Shock Is 1.5

In the following sections, the observed stages in the fragmentation of the large and of the small waterdrop in the airflow behind air shocks that have a Mach number of 1.5 are given. The velocity of the airflow behind the shock is 2.37×10^4 cm/sec for this air-shock velocity.

a. Stages in the Fragmentation of the Large Waterdrop

At the end of 7 μsec after the waterdrop has been struck by the air shock, the high light in it is very bright and seems to contain three points or prongs. See figure 7, picture 1. The pictures with primed numbers in figure 7 are of the high lights in waterdrops before they were struck by an air shock. The waterdrops, the high lights of which are shown in pictures 1′ and 2′, were both contained in the same spark picture. The waterdrop, the high light of which is shown in picture 1′, had just detached from the tip of the hypodermic needle and emerged through the hole in the top of the shock tube. Hence there is a strong probability that this waterdrop was disturbed. The high light of it has some structure. The waterdrop, the high light of which is shown in picture 2′, was close to the bottom of the shock tube and therefore had had some time in free fall in which

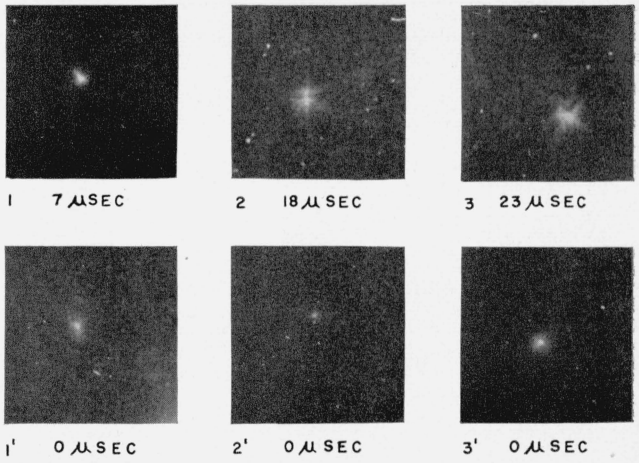

FIGURE 7. *Magnified views of the high light in waterdrops at various time intervals after they were struck by an air shock.*

Mach number of the air shock was 1.5. Pictures with primed numbers are of drops that were not yet struck by an air shock.

to recover from disturbances. The high light in it has no structure. The bright high light of a waterdrop shown in picture 3′ also has no structure. In view of these observations, the structure that appears on the waterdrop high light shown in picture 1 may indicate that the waterdrop in which it existed was disturbed as a result of collision with the air shock, although there is no other apparent indication of it.

The waterdrop high light shown in picture 2, which was taken 18 μsec after the air-shock-waterdrop collision, consists of two hazy pinpoints of light that are close together but that are entirely distinct. Each of these pinpoints of light consists of prongs and gives the appearance of a star. The waterdrop high light shown in picture 3, which was taken 23 μsec after the air-shock-waterdrop collision, is very large and diffuse and may consist of two high lights that are merged or partially superimposed. The diffuse high light is surrounded with spikes or prongs.

In a picture taken 27 μsec after the collision of the air shock with the waterdrop the high light in the drop was so dim that on first examination it was missed entirely. No picture was made in the time interval between 27 μsec and 57 μsec. The picture taken 27 μsec after the collision is the last picture in which any evidence of a high light can be seen in the waterdrop; it is the last picture in which the waterdrop shows no visible sign of distortion, or of reaction to its environment in the airstream behind the shock, or of reaction to having been struck by the air shock itself. In section 3.1.a, it was noted that in the case of large waterdrops that were struck by air shocks having a Mach number of 1.3, a high light could be detected in the drop up to 84 μsec after the air-shock-waterdrop collision. These times after the collision at which the high light may be said to have vanished determine curve A in figure 8 in which the time required to produce comparable stages of fragmentation is plotted against the Mach number of the shock.

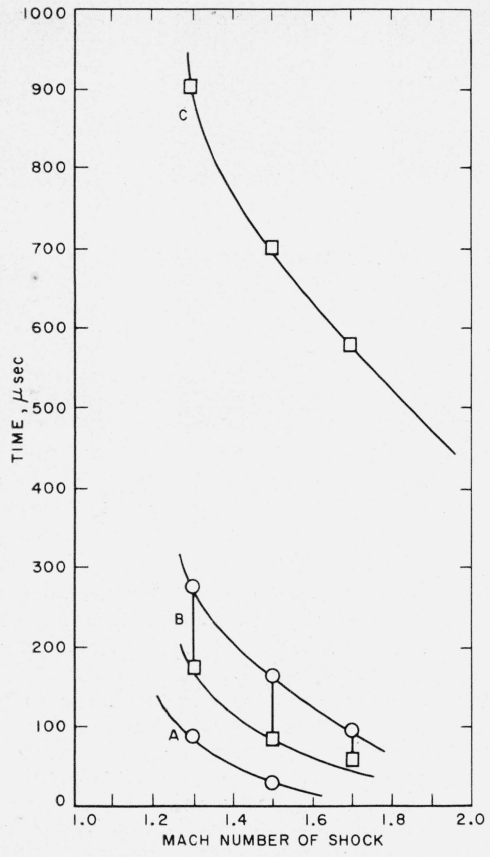

FIGURE 8. *Time to produce comparable stages of fragmentation.*

○ large waterdrop; □ small waterdrop. A, Time at which high light vanishes; B, time to produce a mist cone having a width-to-length ratio of 1 to 3; C, time to produce a trace of mist only.

In a picture taken 57 μsec after the air-shock-waterdrop collision, the waterdrop has no high light at all, and there is no high light in any of the pictures of waterdrops that were taken at longer intervals of time after the collision. The windward face of the waterdrop shows slight evidence of corrugation; mist is emanating from points on the leeward face and from the ends of the major axis of the ellipsoid. A second drop that appears in the picture taken at this interval of time after the collision has two point protrusions at the upper end of the major axis of the ellipsoid and one point protrusion at the lower end of it. These pointed protrusions are bent in the direction of the airflow, and a trail of mist extends into the airflow at the leeward side of the drop from each of them. The production of water mist must, therefore, have started sometime in the 30-μsec interval between 27 and 57 μsec after the collision of the waterdrop with the air shock. The disappearance of the high light may accompany a radial flow of the drop in all directions perpendicular to that of the airflow behind the shock. Such a radial flow of the drop, which was observed in the case of waterdrops struck by air shocks having a Mach number of 1.3 (see section 3.1.a), would destroy its ability to act as a lens for the collimated light in which the radial flow is viewed edge-on.

Because radial flow and production of mist occurred at slightly under 100 μsec for large waterdrops that were struck by air shocks having a Mach number of 1.3, and occur sometime between 27 and 57 μsec after the collision for the same size waterdrop that is struck by an air shock having a Mach number of 1.5, it would appear that an increase of 0.2 in the Mach number of the shock in this velocity range may have caused these phenomena to occur about 50 μsec sooner.

A view of the waterdrop at the end of 59 μsec after collision with the air shock is shown in figure 9. Very small irregularities or bumps can be detected on the windward face, and brushlike structures of mist extend out of the leeward face. The mist has been swept into a stubby, somewhat conical, structure in the airflow downstream beyond the leeward face of the waterdrop. Pictures 2, 3, and 4 of figure 9 show how the corrugation of the windward face of the drop increases with time elapsed since the air-shock-waterdrop collision. They will be referred to in chronological order.

At the end of 94 μsec after the collision of the air shock with the waterdrop, the drop is distinctly flattened against the airflow. See figure 9, picture 2, and figure 10, picture 1. The windward face is strongly corrugated. Brushes of mist extend from points all over the profile of the leeward face, but the largest and most dense are at the top and bottom of the drop as it appears in the pictures.

The mist has been blown into a conelike structure downstream beyond the leeward face of the drop. Pictures of waterdrops taken 97, 98, and 118 μsec after the air-shock-waterdrop collision are very similar in appearance to that shown in figure 10, picture 1, except that the mist cone becomes denser and longer with time elapsed since the collision. At the end of these time intervals after the collision, the leeward face of the drop appears essentially straight, while the windward face is curved and strongly corrugated.

At the end of 159 μsec after the air-shock-waterdrop collision, the contour of the remaining portion of the drop has taken on a distinct quarter-moon shape in which the horns of the quarter moon are on the leeward face and are pointed downstream. See figure 10, picture 2. Mist seems to be spraying from the leeward face in distinct streams, and the mist-cone extending downstream from the leeward face has grown in size and has a width-to-length ratio of about 1 to 3. The closest approximation to this degree of fragmentation for the case that the Mach number of the shock was 1.3 is that which is observed 273 μsec after the air-shock-waterdrop collision. Hence the lag of the lower over the higher velocity shock for producing this degree of fragmentation is 114 μsec. See curve B of figure 8. Pictures of waterdrops taken at the end of 168, 209, 222, and 242 μsec after collision of the air shock with waterdrops are similar in appearance to that shown in figure 10, picture 2, except that the mist-cone is longer and denser. The windward face continues to appear highly corrugated. See figure 9, picture 3.

At the end of 280 μsec after the air-shock-

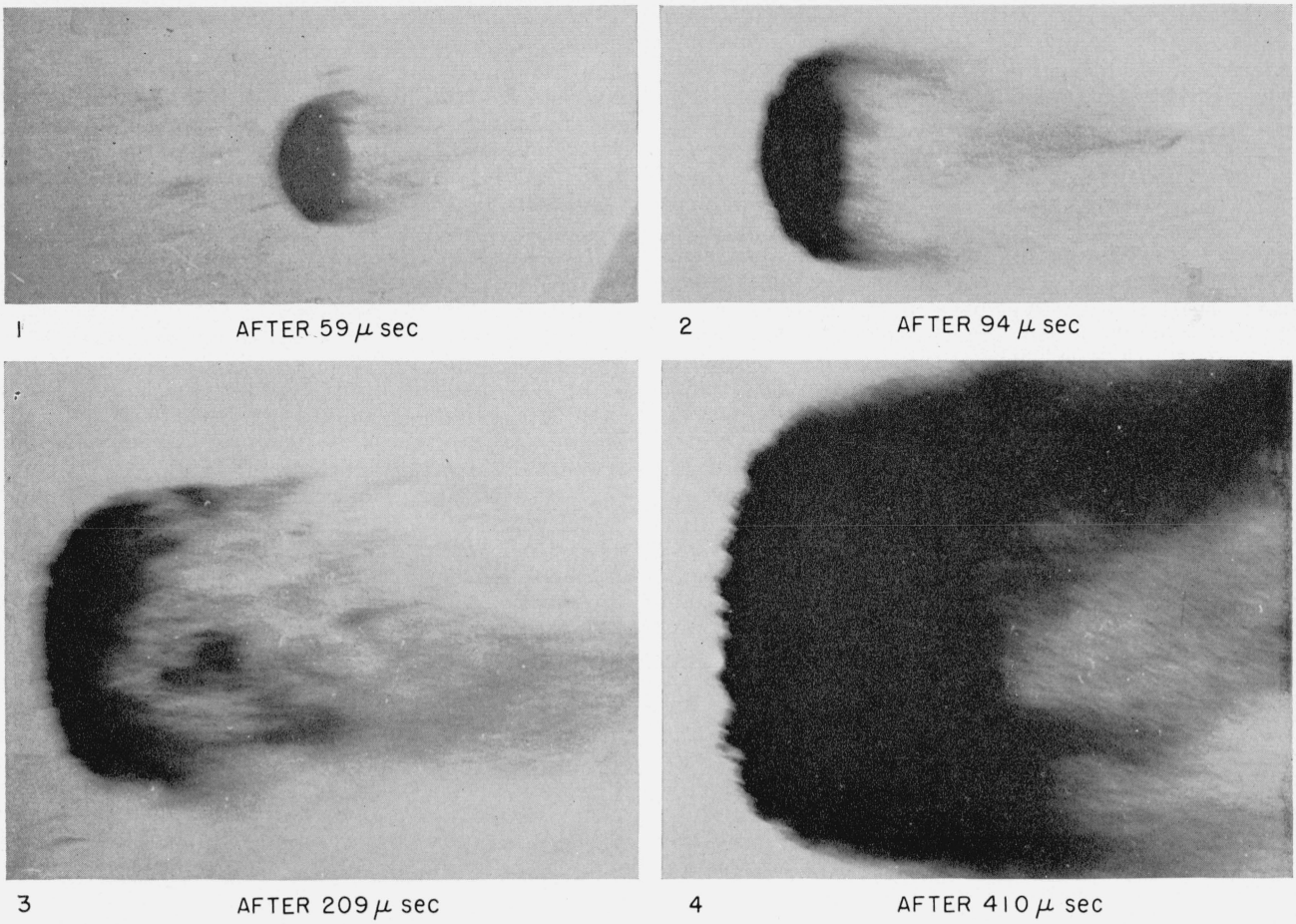

FIGURE 9. *Increase in corrugation of the windward face with time elapsed since the air-shock-waterdrop collision.* Mach number of the shock was 1.5.

waterdrop collision the windward face appears very fringy and the mist extending from the leeward face is hairlike and curled by the turbulence in the wake downstream. See figure 10, picture 3. The remaining portion of the drop is mushroom shaped and is bent at an angle to the airflow. In a picture taken 299 μsec after the collision, the corrugations on the windward face appear to be sharply pointed. In a picture taken 336 μsec after the collision, distinct sections of the remaining part of the drop appear in the mist cone extending downstream from the leeward face.

At the end of 410 μsec after collision of the waterdrop with the air shock, the corrugations of the windward face of the drop are distinctly pointed and appear to be tufted with mist. See figure 9, picture 4, and figure 10, picture 4. However, here, as in all similar appearances at shorter times since the collision, there does not seem to be an orientation of the pointed protrusions on the windward face with the radial flow about the stagnation point. If these pointed protrusions are the crests of waves, or centers of any kind for mist production, the mist emanating from the separate points must be of such low density that it does not show in the photographs. The crests or pointed protrusions also do not appear to be bent in the direction of the airflow from the stagnation point in the center of the windward face. In figure 10, picture 4, a dense hood of mist appears to extend downstream from the leeward face.

In a picture taken 501 μsec after the air-shock-waterdrop collision, the hood of mist that extends downstream from the leeward face is longer. In this picture, the pointed protrusions from the windward face are also longer and there is some sag of the windward face itself which may indicate that the remaining part of the drop is no longer a coherent structure and may possibly consist of mist. In a picture that was taken 589 μsec after the collision, the windward face of the drop has definitely slumped in the wind direction, and in picture 5 of figure 10, which was taken 667 μsec after the collision, this state of affairs is even more marked. A photograph taken 764 μsec after the collision is shown in figure 10, picture 6. Dense spots of mist with corrugated windward faces remain. The trail of mist has spread into a diamond-shaped structure.

In summary, the effect of an increase in the Mach number of the shock from 1.3 to 1.5 appears to be not only a shortening of the time required to bring about the various stages of fragmentation, which was to be expected from the graphs of the flattening

of the waterdrop and of the drift velocity of it in the airstream behind the shock, but also a much more copious production of water mist and of turbulence in the wake downstream behind the waterdrop.

b. Stages in the Fragmentation of the Small Waterdrop

The stage of fragmentation of the 1.4-mm-diam waterdrop shown in figure 11, picture 1, appears to be about the same as that of the 2.7-mm-diam waterdrop shown in figure 10, picture 2. In each case, the remaining part of the drop is bent into a quarter moon with the horns of the quarter moon, which are on the leeward face, pointing downstream. The width-to-length ratio of the mist cone, which is about 1 to 3 in each case, also indicates that these are about comparable stages of fragmentation. The time-after-collision that was required to produce this stage of fragmentation for the 2.7-mm-diam waterdrop is 80 μsec longer than that required to produce the similar stage of fragmentation for the 1.4-mm-diam waterdrop. This may be compared with the time interval of about 100 μsec by which the large waterdrop lagged behind the small waterdrop in reaching a somewhat similar stage of fragmentation when the Mach number of the shock was 1.3. See section 3.1.b and curve B of figure 8. The fact that the lag becomes smaller when the Mach number of the shock is increased may point to the existence of a shock velocity at which the effect of a size difference in the waterdrop is unimportant. Comparison of the pictures of figure 10 with those of figure 11 shows that at the time the 1.4-mm-diam drop is reduced to mist, the windward face of the 2.7-mm-diam waterdrop has just begun to sag in the wind direction.

3.3. Mach Number of the Shock is 1.7

To produce air shocks that had a Mach number of 1.7, a high-helium pressure was required. For safety, the pressure chamber of the shock tube, which was already reinforced with armor plate, was laced with cord. Even with this precaution, however, it was considered inadvisable to take a large number of pictures at this air-shock velocity with the shock tube that was used, and only a sampling was taken over the range of time-after-collision that was explored at the lower shock velocities. The velocity of the airflow behind a shock that has a Mach number of 1.7 is 3.16×10^4 cm/sec.

a. Stages in the Fragmentation of the Large Waterdrop

The state of fragmentation of the 2.7-mm-diam waterdrop 55 μsec after it was struck by the air shock is shown in figure 12, picture 1. Although the head of water of the drop is obscured by the fiducial marker, it is evident that the drop is already copiously emitting water mist. The state of fragmentation of the 2.7-mm-diam waterdrop 91 μsec after it was struck by the air shock is shown in figure 12, picture 2. The stage of fragmentation shown here is almost the same as that which resulted 159 μsec after a waterdrop of the same size was struck by an air shock that had a Mach number of 1.5. See figure 10, picture 2. The difference in the times required to produce this comparable stage of fragmentation is 68 μsec. Because the lag for the shock that had a Mach number of 1.3 over the shock that had a Mach number of 1.5 to produce a similar degree of fragmentation was 114 μsec, it can be seen that the reduction of the time required becomes smaller as the velocity is increased. The time required to produce this stage of fragmentation is plotted in curve B of figure 8.

From a comparison of the pictures of figure 12 with those of figure 10 it can be seen that the stage of fragmentation of the 2.7-mm-diam waterdrop was always much more severe when the Mach number of the shock was 1.7 than for comparable times after the air-shock-waterdrop collision when the Mach number of the shock was 1.5. The appearance of the waterdrop in figure 12, picture 5, about compares with its appearance in figure 10, picture 5, and it can be concluded that at the end of about 430 μsec after collision with a shock that had a Mach number of 1.7, a 2.7-mm-diam waterdrop was reduced to a cloud of mist. The difference in time after the collision for the two pictures is about 200 μsec. Figure 12, picture 6, at the end of 594 μsec after collision of the 2.7-mm-diam waterdrop with a shock that had a Mach number of 1.7, shows a far greater degree of dissipation of the mist that is left of the drop than does figure 10, picture 6, at the end of 764 μsec after collision of the 2.7-mm-diam waterdrop with a shock that had a Mach number of 1.5.

b. Stages in the Fragmentation of the Small Waterdrop

The stage of fragmentation acquired by the 1.4-mm-diam waterdrop 53 μsec after collision with a shock that had a Mach number of 1.7 about compares with its stage of fragmentation 79 μsec after collision with a shock that had a Mach number of 1.5. See figure 11, picture 1. The difference in the time required to attain this stage of fragmentation in the two cases is about 25 μsec. The points are plotted in curve B of figure 8. The 1.4-mm-diam waterdrop is found to be in more advanced stages of fragmentation than at comparable times after the air-shock-waterdrop collision when the Mach number of the shock was 1.5. In a picture taken 574 μsec after collision of the 1.4-mm-diam waterdrop with an air shock that had a Mach number of 1.7, the state of fragmentation is about the same as that in a picture taken 696 μsec after collision of the 1.4-mm-diam waterdrop with an air shock that had a Mach number of 1.5.

3.4. Observed Dependence of the Fragmentation Time on the Diameter of the Drop and the Velocity of the Shock

Because the fragmentation of waterdrops has been observed in this study at only three air-shock velocities for two waterdrop sizes, the amount of generalization as to the effect of the diameter of the drop and the velocity of the shock on the fragmentation time which it is possible to make is limited. In

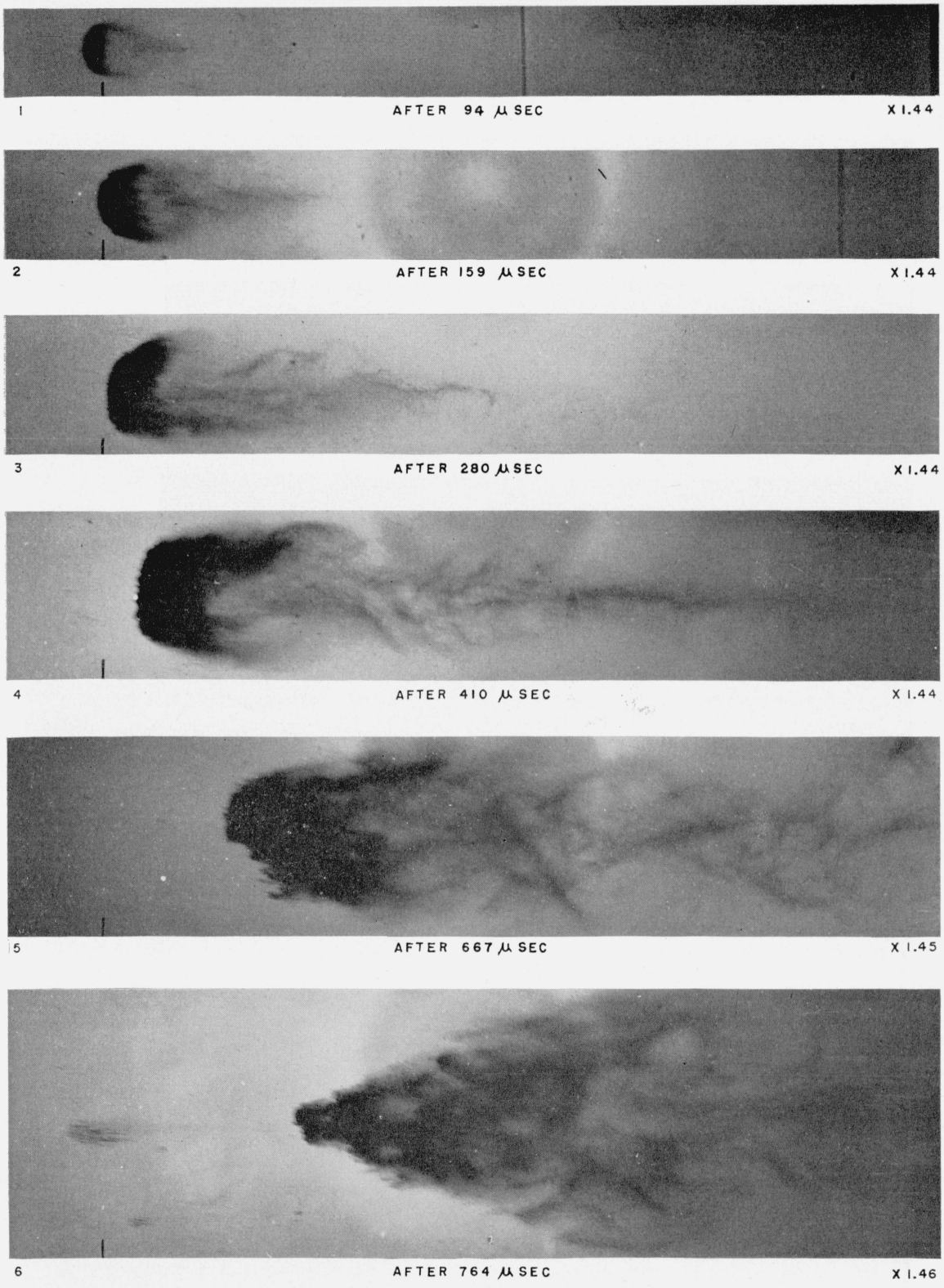

FIGURE 10. *Stages in the fragmentation of 2.7-mm-diam waterdrops.*

Mach number of the air shock was 1.5.

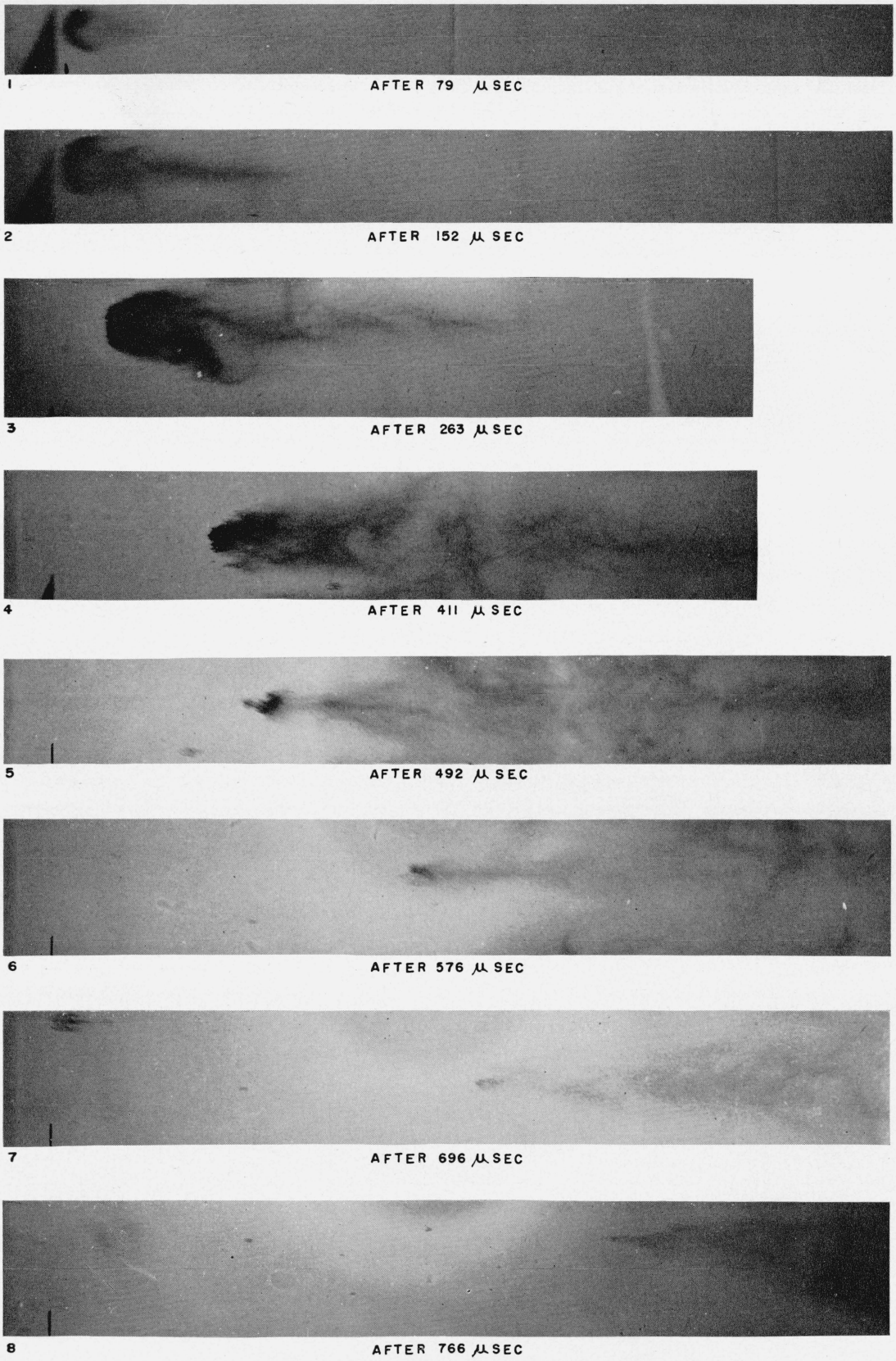

FIGURE 11. *Stages in the fragmentation of 1.4-mm-diam waterdrops.*

Mach number of the air shock was 1.5. × 1.46.

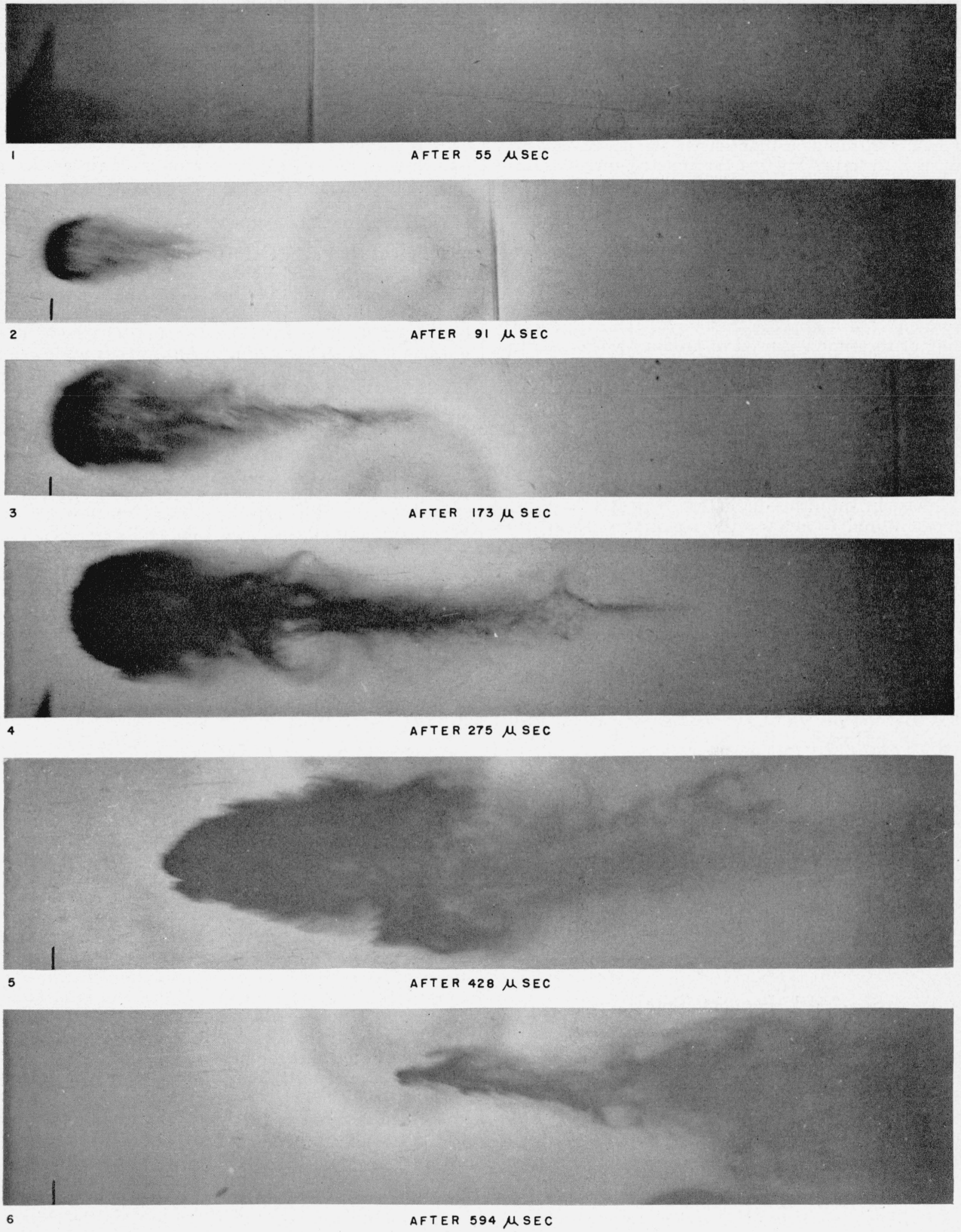

FIGURE 12. *Stages in the fragmentation of 2.7-mm-diam waterdrops.*

Mach number of the air shock was 1.7. × 1.44.

several instances in section 3 a comparison was made of the time required to produce a comparable stage of development in the course of the fragmentation of the waterdrops. The required time for three of these stages of development is plotted against the shock velocity in figure 8. Curve A in figure 8 gives the time required to extinguish the high light in the large waterdrop as a function of the shock velocity. Curve B in figure 8 gives the time required to form a cone of mist having a width-to-length ratio of 1 to 3 downstream from the leeward face of the disintegrating waterdrop as a function of the Mach number of the shock. Data for both the large and for the small waterdrop are given for this stage of fragmentation, and horizontal tie-lines have been drawn between the large-drop and the small-drop values. From curve B it appears that the increment of shortening of the time required to produce this configuration that results on replacing the large waterdrop with the small waterdrop (reduction of the diameter by a factor of 2) is about the same as that which results when the Mach number of the shock is increased by 0.2 in the range of 1.3 to 1.7; that is, a change in the Mach number of the shock is more effective in the rate of waterdrop fragmentation than a change in the drop diameter. Curve C gives the time required to reduce the small waterdrop completely to a trail of mist as a function of the Mach number of the shock. Visual extrapolation of these curves indicates that complete reduction of a small waterdrop to mist may occur within a time interval of the order of 100 μsec when the Mach number of the shock is as high as 3.

4. Mechanism of the Fragmentation of Waterdrops as a Result of Collision With an Air Shock

The data reported in section 3 show only the variation of fragmentation time with drop size and with shock velocity for drops of water in the velocity range that was investigated. The effect of changing the surface tension, viscosity, and density of the liquid of the drop was not explored. Therefore, the information available for deducing the mechanism by which fragmentation occurred is limited. However, in this section, an attempt is made to interpret the observations that were reported in section 3.

4.1. Reaction Time

The 2.7-mm-diam waterdrop showed no visible change in shape immediately after it was struck by an air shock that had a Mach number of 1.3 and, in fact, it existed in the airstream (499 ft/sec) that was flowing behind the shock for nearly 90 μsec before it showed a visible response by change of shape. See section 3.1.a. This behavior is in agreement with the idea that a reaction time is associated with every conceivable movement of matter. During the reaction time, the signal for movement is received and the mechanism of movement is set into operation. An aggregate of molecules of any kind is a coupled system and this is especially the case with water because of the high degree of hydrogen bonding to which it is subject. Therefore it can be expected that the reaction time should be shorter the smaller the mass of water that is involved (drop size) and the stronger the signal for flow that is given (velocity of the shock and of the airflow behind it). This is in agreement with the observed response of two waterdrop sizes after collision with air shocks of three different velocities. See section 3.

4.2. Changes in the Appearance of the High Light

Although the shape of the waterdrop was apparently unaffected for short times after the air-shock-waterdrop collision, the high light in the waterdrop after the collision was noticeably different from the high light in an undisturbed drop. The high light in each of the pictures of waterdrops that were taken after the drop had been struck by the air shock, but before it had shown a visible response by flow, consists of a starlike cluster of prongs or points of light. In some cases, the high light is a double star. See figure 7. It was pointed out in section 3.2.a that the high light in a waterdrop that had been disturbed to the extent of breaking away from the tip of the hypodermic needle and then passing through the hole in the top of the shock tube had some structure in it. The high light in a drop that had fallen freely for several inches, which was contained in the same spark picture, was only a circular pinpoint of light. It seems reasonable to suppose that the structure on the high light is the result of some disturbance of the drop.

The time, τ_n, required for a complete oscillation of a liquid drop for the nth spherical function has been found by Rayleigh [5] to be

$$\tau_n = 2\pi\sqrt{\frac{\rho r^3}{T[n(n-1)(n+2)]}} \tag{25}$$

where r is the radius of the drop; ρ, T are the density and surface tension, respectively, of the liquid of which it is composed. See reference [5], article 364, Vibration of Drops. According to Lenard [6] the case $n=1$ results in no motion, that is, the shape of the drop is spherical; the case $n=2$ is that of the slowest vibration and represents deformation into what is close to an ellipsoidal shape; the cases $n=3$, 4, . . . correspond to more rapid partial vibrations toward the ellipsoidal shape which are anharmonic because their periods do not have a rational relation to the period of the ellipsoidal deformation. A cross section of the solid shapes corresponding to $n=1$, $n=2$, and $n=3$ is in each case a circle when the cut is taken perpendicular to the axis of symmetry. A cross-sectional cut from these shapes taken parallel to the axis of symmetry is a circle for the case $n=1$, an ellipse for the case $n=2$, and a pear shape for the case $n=3$. Models of these shapes were molded of Plasticine and glass models of them were made.[3] Spark pictures of some of these models were taken. Inferences drawn from these pictures must be qual-

[3] These models were made by L. Testa of NBS glassblowing shop.

ified by the fact that the models were about three times larger than the real waterdrops and that they were photographed in the center of the shock-tube window rather than at the extreme left of it as the real waterdrops were so that the optical system was not equivalent.

A high light could be seen in the picture of the glass ellipsoid when viewed through the end and when viewed through the side; it was, in each case, less symmetric than the high light in the picture of the glass sphere. The high light in the picture of the glass ellipsoid that was viewed from the side contained a dim structure somewhat similar to the prongs of light seen on the high lights in pictures of waterdrops that had been struck by an air shock, but it was very much less pronounced. A very dim pinpoint high light that had no structure could be seen in the enlarged end of the pear shape in a picture of this glass model that was viewed from the side; an end view of the glass pear-shaped model was not made. Very little can be concluded from the pictures that were taken of these models; however, a calculation of the period of vibration for the 2.7-mm-diam waterdrop using eq (25) gave the result: for $n=2$, $\tau_2=0.014$ sec; for $n=3$, $\tau_3=0.007$ sec. Because the appearances that were observed in the high lights of waterdrops that were struck by air shocks were all realized in times of less than 100 μsec, it is out of the question to ascribe their existence to oscillations of the waterdrop to these shapes.

In the spark picture of the opaque spherical model that was made of Plasticine, there was no high light, but in the spark picture of the spherical model that was made of glass there was a central pinpoint of light. That the high light is formed by transmitted rather than by diffracted light can be inferred from this observation; the inference must be qualified by the fact that the optical system was not equivalent. If the observed high lights are produced because the waterdrop acts as a lens to the light from the spark, a sharp circular pinpoint of light will form at the focus of the water sphere if the sphere is essentially undeformed. Two modifications of the water sphere that would be capable of causing prongs of light at its focus are the existence of surface ripples and changes in the density of the water of the drop. Either one or both of these disturbances could be caused by the air-shock-waterdrop collision. The passing of the air shock over the waterdrop could conceivably result in microscopic ripples on the surface of the waterdrop; it is also possible that a pulse of compression may be initiated in the waterdrop over the time interval from the first instant that the air shock strikes the center of the windward face of the drop until it passes the center of the leeward face. It would be very difficult to distinguish between these two possibilities even with glass models that were the same size as the waterdrops and that were photographed in the same optical system.

The existence of some structure on the high light of the waterdrop shown in figure 7, picture 1′, indicates that the effect can be produced by ripples alone. This waterdrop was only disturbed to the extent of having just broken away from the hypodermic needle and of just having passed through the hole in the top of the shock tube. It would seem that the possibility of density differences in this drop is remote in comparison with the possibility of surface ripples which should have formed when the residue of the stem of water that was produced as the drop broke away from the hypodermic needle was drawn into the drop under the force of surface tension. The structure on drops that were struck by air shocks is very much more pronounced, however, especially at times after the collision that were of the order of 20 μsec. This could be construed to indicate that density differences may play some role.

The pictures in figure 7 show that while the waterdrop appears to be quiescent during the first 100 μsec after the air-shock-waterdrop collision, it is responding to the collision blow.

4.3. Windward Face Remains Spherical; Leeward Face Becomes Flat

Although the windward face of the 2.7-mm-diam waterdrop was essentially undeformed at the end of nearly 100 μsec after the collision with an air shock that had a Mach number of 1.3, the leeward face appeared flat at the end of 93 μsec after the collision. See figure 3. It has been pointed out [7,8] that a large air bubble rising in water is spherical on top, that is, has a spherical leading surface in the direction of motion, but is flat on the bottom. Taylor [7] has postulated that this shape results as the pressure due to the hydrodynamic flow around the bubble exactly neutralizes the variations in pressure due to gravity at all points on the upper surface of it. The Bernoulli equation is

$$p+\tfrac{1}{2}\rho v^2+\rho gz=\text{constant}, \qquad (26)$$

where p is the pressure, v is the flow velocity, ρ is the density of the liquid, and z is an axis of the coordinate system which is taken in the direction of rise through the liquid. The stagnation point of the flow of liquid around the rising bubble is at the center of its spherical leading surface. Here z is at a maximum but v is zero. If points are considered along any of the streamlines that run radially from the stagnation point around the surface of the bubble, z decreases and v increases. Taylor [7] thought that the net effect is that the second and third terms of eq (26) cancel so that the pressure along a streamline remains constant, that roughly the flat bottom of the bubble occupies the plane at which the pressure on the upper surface is equal to the pressure at the same level far from the bubble, and that surface tension plays no part in producing the observed shape.

Taylor [7] applied the same theory to the shape that should be assumed by a liquid drop in a high speed air blast for the case that the surface of the drop does not disintegrate. On this picture the forces acting to accelerate the waterdrop in the direction of the airflow replace the force of gravity. It is noteworthy in this connection that there is no

apparent drift of the waterdrop during the time interval during which the flattening of the leeward face of the waterdrop is observed. See figure 6, A and B. It is possible, however, that a very small drift does occur.

4.4. Formation of Mist

In deducing a mechanism for the origin of the mist which is observed downstream from the leeward face of fragmenting waterdrops after the air-shock-waterdrop collisions, it is essential to account for all the details that can be observed. The mist appears to emanate from the leeward face of the waterdrop, while the remaining portion of the waterdrop itself remains essentially intact. The mist may, however, actually form on the windward face of the drop and be carried around the drop by the airflow, or it may form at the periphery of the drop between the windward and leeward faces. Viewed from the side, the mist structure has its greatest density at the top and bottom for relatively short periods after the air-shock-waterdrop collision. If a hoop or circle of fringe is viewed edge-on, the observer sees a straight line of fringe with maximum density at either end. In the light of these observations the cone-shaped structure of mist that forms downstream from a fragmenting waterdrop is a hollow funnel. In the case of the 2.7-mm-diam waterdrop, no mist was produced up to 100 μsec after the collision when the Mach number of the shock was 1.3. See figure 3. As the air-shock velocity was increased, the mist formed sooner and more copiously; as the waterdrop diameter was decreased the mist also formed sooner. In the following sections, possible sources of the mist are considered; in the final section an evaluation of the most probable of the sources is made.

a. Vaporization

The appearance of the water mist suggests the possibility of a hot-water-vaporization-to-form-steam mechanism. As soon as the air shock passes the waterdrop, the waterdrop exists in the airstream that is flowing behind the shock. The temperature in this airstream is considerably higher than the room temperature of the undisturbed air in front of the shock. For air shocks having Mach numbers of 1.3, 1.5, and 1.7, the temperature in the airstream behind the shock is 84° C, 123° C, and 165° C, respectively, if the initial temperature was 27° C. See table 1. There is, furthermore, an elevated temperature at the stagnation point of the airflow in the center of the windward face of the waterdrop. This temperature was found in section 2.6 to be 95° C when the air shock had a Mach number of 1.3. In section 2.5.a, the pressure at this point for the same air-shock velocity was found to be 1.99×10^6 d/cm^2 (1.96 atm). Because water boils at 100° C at 1 atm, no vaporization would be expected on the windward face in terms of an equilibrium picture. On the leeward face, the pressure is reduced only to 1.69 atm and the temperature on this face is 80° C when the air shock has a Mach number of 1.3. See sections 2.5.b and 2.6. Consequently, in terms of the equilibrium picture, no vaporization would be expected on this face either. Although equilibrium conditions have certainly not been reached in the order of 100 μsec, which is the time after the air-shock-waterdrop collision at which mist was first seen, it seems doubtful if a hot-water-to-form-steam mechanism is the source of it.

To determine whether or not clouds of mist form behind a waterdrop that is falling through a layer of hot air, high speed moving pictures were taken of incidents of this kind. Glass windows were installed in the ends of a heavily insulated electric oven which contained a small electric fan to distribute the hot air. Light from a carbon arc was passed through a collimating lens and then through the windows of the oven. Drops of distilled water were allowed to fall from the large-bore hypodermic needle through a hole in the top of the oven located at the focal point of the lens of the 15,000-frame/sec camera that was used to take pictures of the falling drops. The camera was placed at the end of the oven opposite the arc light so that the pictures of the falling waterdrops were shadowgraphs.[4]

Moving pictures of waterdrops were taken both after a short and after approximately the longest possible distance of fall through the oven (6.1 in.) at oven temperatures of about 80° C, 125° C, 160° C, and 260° C. Still enlargements of consecutive frames from the movie films show that no cloud of mist was trailing the falling drop at any of the oven temperatures for which observations were made either for the short or for the long distance of fall through the oven. Because the time of fall of the waterdrops through the oven was of the order of tenths of a second, it was concluded from these pictures that the time required for heat transfer to and subsequent vaporization of water from the surface of a falling drop is too long to account for the formation of the water mist which was detected 100 μsec after a waterdrop was hit by an air shock that had a Mach number of 1.3. Consequently a hot-water-vaporization-to-form-steam mechanism based on the elevated temperature of the air that is flowing past the waterdrop after it has been struck by the air shock cannot be a correct explanation of the water mist that emanates from it.

b. Mechanical Origins

The circumstances under which the water mist is formed suggest that the mechanism by which it is produced is mechanical. Mechanisms in this category are that by which mist is produced as a result of sound waves, the stripping off of a surface layer of water by the rapid airflow around the drop, and the breaking of the crests of surface waves. These possible mechanisms are discussed and evaluated below.

(1) *Sound Waves as a Source of Water Mist.* It is known that liquids can be converted to mist by sound waves [9]. In the case of liquids of low viscosity, at a liquid-air interface, the forces in play drive the liquid into the air in the form of a spray

[4] Lee Dunlap and W. K. Stone assisted in these experiments.

of minute droplets to form a fog [9]. Because sound waves may be initiated in a waterdrop that has been struck by an air shock, it is possible that the mist that is carried downstream from waterdrops that have been struck by an air shock could have this origin.

Two experiments were made by Martin Greenspan and Max Swerdlow of the Bureau, to observe directly the reduction of a liquid to mist by means of ultrasonic waves. Drops of ethyl alcohol were placed on the bottom of a glass vessel which was then set into rapid vibration by an oscillating crystal. Clouds of white fog rose from the drops of alcohol and the small drops of alcohol emitted mist more copiously than the large drops did.

A second demonstration of the effect was made using a powerful Crystalab Ultrasonorator. This instrument consists essentially of a crystal that is driven at high frequency while it remains submerged in an oil bath. A beaker containing a small amount of water was placed so that the bottom of it was in contact with the surface of the oil. When the crystal was set into oscillation, a small and rapidly fluctuating mound of water rose above the surface of the water in the beaker. It gave the appearance of what might be expected if a water nozzle, located below the surface of the water in the beaker and pointed toward the surface, were delivering a jet of water through the surface. Periodically dense clouds of mist rose from the head of the water jet. A moving picture was taken of the phenomenon. The fluctuating action of the jet on the surface of the water can be seen in a still enlargement of consecutive frames from this movie. Mist was thrown off wildly in various directions as the jet of water thrashed about. To establish whether this mist is produced mechanically, or as a result of local heating, a small quantity of Ascarite was added to the water in the beaker. A piece of pink litmus paper that was held in the mist underwent a definite though slight color change. This would have been impossible if the mist had consisted of distilled water. However, it seems that the presence of hydroxyl ion in the vapor above the water could be accounted for as a result of cavitation in the water itself [5] which destroys the conclusiveness of this evidence that the origin of the mist was mechanical.

In the case of the evolution of water mist from waterdrops after they have been struck by an air shock, it seems that the actual process could consist of a spalling of water from the free surface of the leeward face of the drop after a pressure pulse reverses there in tension because water, except under very special conditions, has very little tensile strength. On the other hand, it could consist of the breaking of the crests of waves that may be produced by the successive reflection of an initial pressure pulse from the two faces of the drop. These two possibilities are discussed in the following paragraphs.

The spalling mechanism is briefly as follows [10]. When a pressure pulse of steep front reverses in tension at a free surface, interference occurs at first between the incident compressional wave and the reflected tension wave. Tension increases as the reflected wave moves away from the surface. When the medium in which the wave is moving is no longer able to withstand the tension, fracture occurs, and a scab or thin layer is thrown off the free surface. Because water has such low tensile strength, this layer, in the case of a water scab, should be vanishingly thin. It is possible for a second scab to form as the remainder of the pressure pulse reflects in tension from the fresh surface produced by the formation of the first scab. In this way, multiple scabbing can be accounted for [11]. These scabs or thin sheets of water would break up into droplets of very small size [12].

Compressional waves which may be initiated on the windward face of the waterdrop at the instant that the air shock strikes it would reflect in tension from the leeward face of the drop which is a free surface. After the reflected tension wave returned to the windward face of the drop, it would reflect there as a compressional wave because the windward face is also a free surface (reflection occurs with change of sign at a free surface). The process of successive transits of the waves through the waterdrop at the speed of sound in water, and of their successive reflection, would continue until the waves were damped out. The attenuation of sound in water is low.

It has been shown that the thickness of an air shock that has a Mach number of 1.7 is 0.000031 cm. Because this is approximately 1/10,000 the diameter of the waterdrop, the initiation of a pulse of compression in the waterdrop is possible. The amplitude of it may not be large. However, there is no clear evidence of mist formation up to 100 μsec after a 2.7-mm-diam waterdrop has been struck by an air shock having a Mach number of 1.3, although the time that is required for a pressure pulse to make one trip through a 2.7-mm-diam waterdrop at the speed of sound in water is about 2 μsec. There does not seem to be an answer to this discrepancy other than the observation that it is hard to decide just when mist can first be detected in the spark pictures of waterdrops that have been struck by air shocks and that there are periods of quiescence even in the case where water is exposed to ultrasonic waves.

If reflecting waves are the cause of the mist, there should be a more or less even density of mist formation over the whole leeward face of the waterdrop and the mist structure that forms downstream from the leeward face should have its greatest density in the center when it is viewed from the side. However, it can be seen from the spark pictures that for relatively short times after the air-shock-waterdrop collision, the greatest density of the mist structure is not at the center but at the top and bottom as the mist structure is viewed from the side. This certainly seems to indicate that the mist structure is hollow which would lead to the conclusion that the mist is not being formed on the leeward face but, instead, is being formed on the windward face and is being carried around the drop by the airflow or is being formed at the periphery of the drop between the windward and leeward faces. Furthermore, if the reflection of pressure waves as tension waves at

[5] Suggested by Virginia Griffing of the Catholic University.

the leeward face of the drop is the source of the mist, the greatest density of mist formation should occur at short times after the air-shock-waterdrop collision, that is, before the traveling wave has time to become attenuated. However, from the spark pictures of fragmenting waterdrops it appears that the density of mist production increases with time elapsed since the collision incident until quite long periods of time have elapsed. For these reasons it seems very doubtful that the observed water mist is produced from water scabs formed at the leeward face of the waterdrop as a pressure pulse reverses in tension.

It is possible that a pressure pulse may be initiated but that the ultimate effect of its subsequent reflections from the faces of the waterdrop may not be to spall mist from the leeward face of the drop. The successive reflection of the pressure pulse may result in waves on the surface of the drop; the crests of these waves may break, or may be whipped off by the rapid airflow around the drop. Because such waves could form on the windward face of the waterdrop, this view of the function of the pressure pulse, if one is formed in the waterdrop, would be in agreement with the observation that the mist density behind the leeward face is not uniform, but is greatest at the top and bottom when the fragmenting waterdrop is viewed from the side. On this picture the formation of the mist would also be delayed until the waves were set up on the surface of the drop. This would be in agreement with the observation that the mist does not form immediately after the air-shock-waterdrop collision.

(2) *Surface Waves as a Source of Water Mist.* It was pointed out in the preceding discussion that waves may be produced on the surface of a waterdrop as a consequence of a successively reflecting pressure pulse which may have been initiated by the air-shock-waterdrop collision and that these waves may break or that the crests of these waves may be blown off by the rapid airflow around the drop to produce the water mist. It is also possible that surface waves may be produced by the wind that is blowing out radially around the stagnation point in the center of the windward face of the waterdrop and that crests of these wind waves may break or be blown off.

Whatever may be their origin, surface waves certainly appear on the windward face of a waterdrop after it has been struck by an air shock and exists in the high-speed stream of air that flows behind the shock. The development of windward-face corrugations with time is shown in figure 9 for waterdrops that were struck by air shocks that had a Mach number of 1.5. For short times after the collision incident they are only rounded mounds on the surface as in figure 9, picture 2; later they become choppy or sharp-pointed waves as in figure 9, picture 4.

There is some evidence for identifying the waves seen in the profile of the windward face of the waterdrop in figure 9, picture 4, as wind waves. In general, in the presence of gravity two sets of waves are produced by a given wind velocity. It can be seen that very small ripples are superimposed on larger waves in the profile of the windward face of the waterdrop in figure 9, picture 4. The evidence can be further confirmed by calculating the ratios of the values of the allowed wavelengths that capillary waves should have under the experimental conditions and by noting if the observed wavelengths are in approximately this ratio.

The theory of waves produced by wind under the condition that surface tension and the field of gravity are both acting is known [13]. The case being considered here is that a freely falling waterdrop is struck by an air shock in a shock tube. The waterdrop is then accelerated downstream in the rapid airflow in the tube behind the shock. For this case the acceleration due to gravity is negligible in comparison with the horizontal downstream acceleration that, neglecting the drag of the flowing air, is due to the pressure difference between the windward and leeward faces of the drop. For this case the air-water interface is the windward face of the waterdrop and it is perpendicular to rather than parallel with the surface of the earth. The theory for this case is the same as that for waves produced by wind on a body of water under the condition that surface tension and the gravitational field of the earth are both acting. See Lamb, [13], chapter IX, Surface Waves, article 246.

It leads to the equations

$$c_m^2=\frac{2\sqrt{\rho_w-\rho_a}\sqrt{\alpha T}}{\rho_w+\rho_a}, \tag{27}$$

$$\lambda_m=2\pi\sqrt{\frac{T}{\alpha(\rho_w-\rho_a)}}, \tag{28}$$

$$\frac{c^2}{c_m^2}=\frac{1}{2}\left[\frac{\lambda}{\lambda_m}+\frac{\lambda_m}{\lambda}\right], \tag{29}$$

where c is the velocity of the waves, λ is the wavelength, T is the surface tension, ρ_w, ρ_a are the densities of water and of the air flowing behind the shock, respectively, α is the acceleration of the waterdrop in the airflow behind the shock, and the sub-m notation indicates the minimum value of the quantity.

For every value of $c^2/c_m^2>1$, there are two values of λ/λ_m, that is, there are two values of the wavelength as was noted above. Two values of these ratios given by Lamb [13] are: $c/c_m=1.2$, $\lambda/\lambda_m=2.476$ and 0.404; $c/c_m=1.4$, $\lambda/\lambda_m=3.646$ and 0.274. From these ratios, the equations for c_m^2 and λ_m, and taking the average value of α, the slope of the drift-velocity-against-time curve for the time interval up to 400 μsec to be 6×10^6 cm/sec^2 for the case that the Mach number of the shock is 1.5 (see fig. 6, C), and $\rho_a=\rho_2$ for the airflow behind shocks that have a Mach number of 1.5 (see table 1), it is possible to calculate the ratio of the wavelengths that should be observed on the windward face of the waterdrop shown in figure 9, picture 4. From eq (27)

$$c_m=\left[\frac{2\sqrt{1-0.00218}}{1.00218}\sqrt{72(6\times10^6)}\right]^{1/2}=203.6 \text{ cm/sec}$$

and from eq (28),

$$\lambda_m=\frac{2(3.1416)\sqrt{72}}{\sqrt{(6\times10^6)(1-0.00218)}}=0.02179 \text{ cm}.$$

By use of the ratios given above, when c=244.3 cm/sec, λ_1=0.05395 cm, λ_2=0.008803 cm, and when c=285 cm/sec, λ_1=0.07945 cm, λ_2=0.00597 cm. The calculated values of the wavelength, λ, are plotted against the values of the wave velocity, c, in figure 13. The measured wavelength of the coarse waves on the windward face of the waterdrop shown in figure 9, picture 4, is roughly 0.06 cm. From figure 13 the wavelength of the ripples between the coarse waves should be 0.0082 cm. Measurements indicate a value of 0.014 cm.

The evidence seems to indicate that surface waves do form, that two wave lengths exist as is to be expected from theory, and that the ratio of the wavelengths is roughly what should be expected from theory. Waves are observed on the windward face of waterdrops before the waterdrops are accelerated downstream. See figure 9, pictures 1 and 2. Wind waves can form in the absence of a gravitational field; under this condition, however, only one wavelength is to be expected.

(3) *Unstable Waves.* Taylor [7] (see also Lane and Green [14]) suggested that the formation of unstable waves might constitute a mechanism of fragmentation. The crests of the waves may blow off to form droplets. The diameters of the droplets produced in this way are likely to be of the same order as the wavelength of the most unstable wave. For high airflow rates, calculations based on this hypothesis produce much smaller values for the size of the droplets than are found experimentally. Taylor [7] has suggested that it is possible that the discrepancy may result from the fact that the air close to the fluid surface is moving slower than the air outside the boundary layer and is therefore less effective in producing waves.

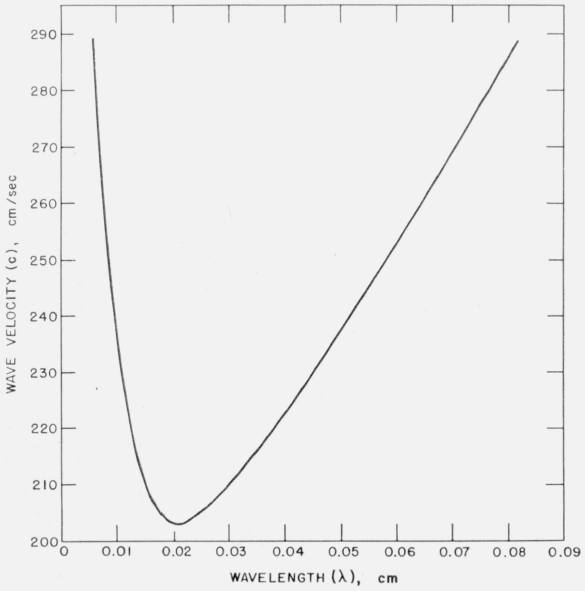

FIGURE 13. *Corresponding values of the wavelength and wave velocity for a water surface that is being accelerated at the average rate of* 6×10^6 *cm/sec*^{2}.

(4) *Stripping of a Surface Layer of Water by the Airflow.* Taylor [7] has considered the possibility that waterdrops may disintegrate in a high-velocity airstream by means of the stripping off of a surface layer of water which then breaks up. Air is flowing radially from the stagnation point on the windward face to the equator of the waterdrop midway between the windward and leeward faces of it. The motion of the air sets the surface layer of the water on the windward face of the drop into motion. This thin moving layer of water spills off the drop at the equatorial belt that separates the windward and leeward faces of the drop and breaks up to form the mist that is observed downstream from the leeward face.

It can be shown (see appendix A) that the total efflux or total loss of volume from the boundary layer per unit time is

$$\frac{dV}{dt}=4\pi r\left(\frac{\rho_a}{\rho_w}\right)^{1/3}\left(\frac{\nu_a}{\nu_w}\right)^{1/6}\sqrt{U_2-W}\sqrt{\nu_w}\sqrt{x} \qquad (30)$$

where ρ is the density, ν is the kinematic viscosity, U_2 is the velocity of the airflow, W is the drift velocity of the waterdrop, and x is a distance along a radius of the windward face of the waterdrop measured from the center of the windward face. The sub-a notation refers to the air and the sub-w notation refers to the water. Taylor [7] used eq (30) to develop an expression that was intended to give the decay of a lenticular drop from the time that it had undergone maximum flattening (see section 4.6) to the time of complete disintegration by means of efflux of liquid at the periphery between the windward and leeward faces and found the condition that the drift velocity, W, should have reached the airflow velocity, U, at the time that complete disintegration was accomplished. He later [14] modified this conclusion. At the time that fragmentation of the 2.7-mm-diam waterdrop was essentially complete, the drift velocity was about 33 percent of the airflow velocity when the Mach number of the shock was 1.5, and about 50 percent of the airflow velocity when the Mach number of the shock was 1.7. See section 4.7. The condition that the waterdrop should acquire the airflow velocity before fragmentation is complete may possibly be realized when the fragmentation of waterdrops in the airflows behind shocks having Mach numbers greater than 1.7 is investigated. Lane and Green [14] report that a 0.5-cm drop of dibutyl phthalate disintegrating in a 3.4×10^4 cm/sec air blast had attained 90 percent of the airflow velocity at the time that the drop was essentially completely fragmented.

Results of the present investigation seem to indicate that a marked reduction in the drag force of a waterdrop occurs between 100 and 200 μsec

after the air-shock-waterdrop collision (see section 4.7). The fragmentation mechanism may be more complicated than was assumed by Taylor [7] when he wrote the expression that was intended to give the decay of a lenticular drop from the time of maximum flattening to the time of complete disintegration by means of the efflux of liquid at the periphery between the windward and leeward faces. It is possible that instead of remaining in the form of a water disk during the disintegration process the water disk is converted to a ring of water when a hole forms at the center of the windward face and that eventually the water ring segments into a chain of water beads. To evaluate surface-layer stripping as a possible mechanism for liquid-drop fragmentation by determining what the drift velocity should be at the time that fragmentation is complete, it is necessary to determine experimentally whether these large changes in the form of the liquid mass that remains of the drop actually do take place. If they do occur, it will be necessary to apply the surface layer stripping mechanism to these forms of the water mass in an equation designed to trace the complete decay of the liquid drop to mist. For a further discussion of this point, see section 4.7. However, there may be a Mach number of the air shock considerably higher than 1.7 for which the airflow behind the shock would have a sufficiently high velocity to reduce the waterdrop radius to zero by a surface-layer stripping mechanism before the complication of hole formation or of segmentation of the remaining water ring would have time to occur.

(5) *Turbulence as a Source of Mist.* Potential flow exists around the waterdrop immediately after the air shock has struck it. This means that there are no vortices in the flow and that the stagnation pressure at the center of the leeward face is equal to the stagnation pressure at the center of the windward face. Vortices will form, however, in a time interval of the order of 100 μsec after the air-shock-waterdrop collision and as the vortices form, the pressure on the leeward face will drop. The vortices themselves may be a source of the water mist, that is, they may gradually eat away the leeward face of the waterdrop.

Because the direction of the airflow in the vortices is toward the equator of the drop, the mist that may be produced as a result of the vortex motion would be carried back toward the equator of the drop before it entered the airflow downstream from the leeward face. This would require that the mist cone should be a hollow funnel as is observed.

The time that is needed for the formation of the vortices would require that there should be a time interval after the air-shock-waterdrop collision in which no mist is formed. This is the case where the air shock had a Mach number of 1.3, but for this air-shock velocity there is no evidence of turbulence in the mist structures that form downstream from the leeward face of the fragmenting drops for any time after the collision incident at which pictures were taken. See figure 4, pictures 1 through 6. On the other hand, in the case of collisions of waterdrops with air shocks that had a Mach number of 1.5, there is already a well-developed mist-cone in pictures that were taken at about 85 μsec after the collision incident (see fig. 10) and in the case of collision of a waterdrop with an air shock that had a Mach number of 1.7 there is a mist structure behind the leeward face of the drop at the end of about 55 μsec. See figure 12. Furthermore, in pictures of waterdrops that were taken at time intervals less than 100 μsec after the waterdrops were struck by air shocks that had Mach numbers of 1.5 and 1.7, there was no evidence of swirling in the mist structure downstream from the leeward face, but in pictures that were taken at the end of longer time intervals after the collision of a waterdrop with air shocks that were moving at these velocities, strong evidence of swirling exists.

These observations seem to indicate that mist can be produced in the absence of vortices, that is, that the mist has an origin other than the vortices. The existence of vortices may, however, contribute to the production of mist after they form. This is in agreement with the observation that the mist density is greater for comparable times after the air-shock-waterdrop collision as the air-shock velocity was increased.

(6) *Most Probable Sources of the Water Mist.* From a consideration of the evidence for and against the various postulated mechanisms for mist production that have just been given, it seems that the most likely mechanisms are those which take into account the effect of the rapid airstream on the waterdrop. The mist that is observed is probably made up of contributions from the whipping off or from the breaking of the crests of waves, from the spill-off at the equatorial belt of the moving boundary layers on the windward face, and from the stripping of water from the leeward face by the vortices that form there in the airflow. It seems unlikely that one of these mechanisms operates to the complete exclusion of the others.

4.5. Radial Water Flow

The start of evolution of water mist from the leeward face of a waterdrop after it has been struck by an air shock is accompanied by the first evidence of a radial flow of water from the drop. The thin sheet of water that is just beginning to move out radially at the equator of the drop appears only as a protrusion from the upper and lower surface of the silhouette of the drop as it is seen in the spark pictures. The gradual development of it over a period of about 70 μsec can be seen in figure 3, pictures 1 through 8, for the 2.7-mm-diam waterdrop after collisions with air shocks that had Mach numbers of 1.3.

To determine the cause of this radial flow, it is necessary to account for all the variations of it with the conditions under which it forms. From the pictures that were just referred to, it is seen that (A) when it is produced as a result of collision of a waterdrop with an air shock it moves out of the drop on a plane that extends through the center of the drop and that is perpendicular to the direction of motion of the air shock that struck the waterdrop. Com-

parison of spark pictures of the large and of the small waterdrop at various times after the air-shock-waterdrop collision shows that (B) the radial flow forms sooner for a small than for a large waterdrop. When the Mach number of the shock is 1.3 the formation time for the 2.7-mm-diam waterdrop is of the order of 100 μsec, but for the 1.4-mm-diam waterdrop it is much less than 75 μsec, because for this size of waterdrop the radial flow is already well developed 75 μsec after the air-shock-waterdrop collision. A comparison of the size of the radial flow with the diameter of the residue of the drop seems to indicate that (C) the radial flow may be larger the smaller the diameter of the drop.

This interesting phenomenon also results if liquid drops are suspended in a sound field. It is very evident, for example, in pictures taken by Hanson, Domich, and Adams [15]. In this case (A′), the radial flow forms perpendicular to the direction of the sound field. For drops of methyl alcohol of different sizes which Hanson, Domich, and Adams [15] suspended in a sound field, only drops having a diameter of 0.0334 cm or less, have the radial flow. The high light in the drops that have the radial flow is completely extinguished whereas the larger drops that have no radial flow have distinct high lights. It is noteworthy that the limiting size of drop that will develop a radial flow in the sound field that was used by Hanson, Domich, and Adams is lower for drops of water than for drops of methyl alcohol because a 0.0315-cm waterdrop suspended in the sound field has a distinct high light and no radial flow. There is no way of knowing (B′) the rate at which the radial flow formed on these drops. However, (C′) among the drops of methyl alcohol that have a diameter of 0.0334 cm or less, the smaller the drop is, the more extensive is the radial flow. A 0.0168-cm drop has a large radial flow, a 0.0334-cm drop has a small radial flow, and 0.0511- to 0.0793-cm drops have no radial flow. Although the sound frequency is not indicated on the picture given by Hanson, Domich, and Adams [15], it appears probable from their discussion that a 50-kc field was used. After these drops were struck by an air blast that had a velocity of 60 ft/sec, the radial flow was blown off the drop and existed as a mist structure downstream from the leeward face of it [15]; this appears to be evidence to indicate that the water mist, which was discussed in section 4.4, had its origin at least partly in protrusions of one kind or another that formed on the surface of the drop. The cause of the radial flow is undoubtedly the same regardless of whether it occurs as a result of collision of a drop with an air shock or as a consequence of supporting a drop in a sound field.

The lowest pressure that occurs around a sphere that is located in an airflow exists in a belt around it that separates the windward from the leeward face. The pressures that were found by Fage [4] to exist at all points from the center of the windward face to the center of the leeward face for a 6-in.-diam sphere in a 35 ft/sec airflow are given in figure 14, B. From these data the low-pressure belt be-

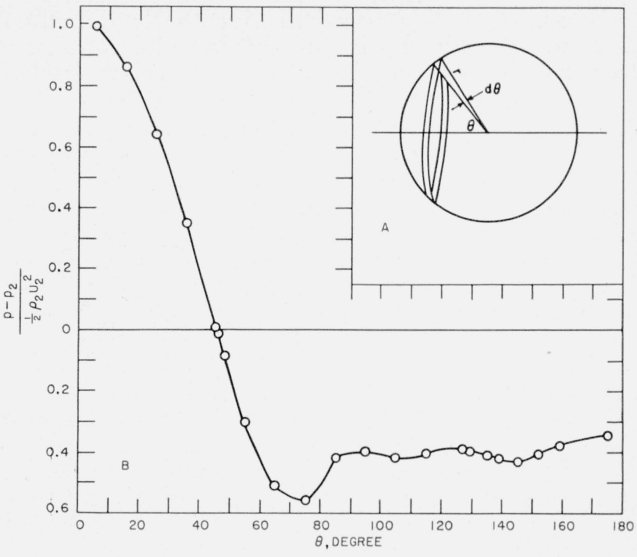

FIGURE 14. *A, Differential area; B, distribution of pressure around a 6-in.-diam sphere in a 35-ft/sec airflow.*

Reynolds number 110,000. Data of Fage [4].

tween the windward and the leeward face exists from 60° to 85°. It can be expected that the high pressures that exist on the windward and leeward faces of a deformable water sphere during the period when potential flow occurs, that is, when the stagnation pressure on the leeward face is the same as the stagnation pressure on the windward face, will drive water out through the low-pressure belt. This water flow, however, occurs throughout the drop and is not restricted to a very narrow zone at the equator. These exterior pressure differences are the cause of the gradual flattening of the drop, which is discussed in section 4.6, but they are not the cause of the very localized thin circular sheet of water that moves out of the equatorial belt of the drop.

It is shown in section 4.6 that a memory of some kind may exist in the water of the drop. This memory may be a pulse of compression. It is seen from figure 3 that an air shock that is moving at supersonic velocity can collide with a waterdrop without producing an immediate distortion of it. However, a layer of water on the windward face of the drop may be given an almost instantaneous acceleration at the instant that the shock wave passes over the drop, that is, a pulse of compression could be initiated. This pressure pulse would move at the speed of sound in water from all points on the hemispherical windward face through the geometrical center of the drop and would be reflected as a tension pulse from the mirror-image points on the hemispherical leeward face of the drop. The center of the drop which is the point of intersection of the reverberating pulse, may be the point where maximum pressure amplitude occurs because maximum superposition occurs there.

The radial flow of water that moves out of a waterdrop that has been struck by an air shock, comes out

on a plane that is perpendicular to the direction in which the air shock was moving and that runs through the center of the drop. Likewise, the radial flow that comes out of a drop of methyl alcohol that is suspended in a sound field also moves out on a plane that is perpendicular to the direction in which the sound pulses strike the liquid sphere and that runs through the center of the drop. This is in agreement with observations (A and A′) cited above. The maximum pressure that would result from superposition of waves would develop sooner in a small waterdrop than in a large waterdrop because the time required for the pressure pulse to make a trip across the drop would be shorter. This would also be the case for pressure pulses set up in waterdrops suspended in a sound field. This is in agreement with observation (B) cited above. Finally, the pressure that would be developed in the center of the drop as a result of collision of the drop with an air shock moving at a given velocity or as a result of a sound field of specified intensity would be capable of driving a radial flow of water a certain distance. Compared with the diameter of the drop, this distance would be larger for a small drop than for a large drop. This is in agreement with observations (C and C′) cited above. If the pressure developed is incapable of driving a water flow to a distance larger than the diameter of the drop itself, no flow would be observed. This is in agreement with the observation that in the case of drops of methyl alcohol that were suspended in a sound field, no radial flow at all was observed on the largest of the drops. To make a comparable statement for waterdrops that were struck by air shocks, it would be necessary to observe the behavior of waterdrops that had a diameter larger than 2.7 mm after they were struck by an air-shock that had a Mach number of 1.3 or to observe the behavior of the 2.7-mm-diam waterdrops after collision with air shocks that have Mach numbers less than 1.3.

On the other hand, it is possible that this radial flow may be produced by instability on the surface of the drop. The airflow, which follows the air shock, blows against the windward face of the drop and water waves are initiated by it. Similarly, there is a periodic movement of air past a liquid drop that is suspended in a sound field and this air movement could have the same effect. The stability of waves on the surface of a liquid drop is a function of their latitude on the sphere with respect to the stagnation point in the center of the windward face which may be considered as a pole. The line of maximum instability is at the equator of the drop and it is possible that surface waves may grow to a very high amplitude at the equator to give the appearance of a radial flow. This would be in agreement with observations (A, A′) cited above.

The growth of an unstable wave on the surface of a spherical body is mathematically an extremely difficult problem. This is especially the case at the later stages of the growth of instability when the radial flow develops. However, from stability theories on simple models, it is to be expected that waves of small wavelength, produced as the result of eigenvibrations, are likely to be associated with small bodies and that, under many circumstances, waves of small wavelengths are more unstable than waves of large wavelengths [16]. Small bodies also respond readily to the influence of an external unsteady field because of their small inertia. This evidence may provide an explanation of observations (B) and (C, C′) cited above.

4.6. Flattening of the Waterdrop in the Airflow

The flattening of the waterdrop perpendicular to the direction of the airflow in the shock tube is the result of the pressure difference that exists around it in the airflow behind the shock. Burgers [17] has accounted for the flattening with time by use of a simple model, namely, that at the instant that the air shock has just passed the waterdrop streamlines converge at the center of both the windward and leeward face of it and the pressure at the center of each of these faces is the stagnation pressure. See appendix B. The outward displacement d at the equator of the drop and perpendicular to the direction of the airflow is found to be given by

$$d=\frac{1}{3}\frac{\Delta p}{\rho r}t^2 \tag{31}$$

where Δp is the pressure difference between either the windward- or the leeward-face stagnation point and points along the equator of the drop, r is the drop radius, ρ is the density of the liquid of the drop, and t is the time. The increase in the diameter of the waterdrop perpendicular to the direction of the airflow is $2d$.

From eq (31) it can be seen that the smaller the waterdrop is, the larger is the increase in its diameter perpendicular to the direction of the airflow for any given time after the air-shock-waterdrop collision. This is in agreement with observation. See section 3.1.b. It appears that with a constant pressure difference between the poles and equator of a liquid sphere, the pressure gradient inside the sphere becomes larger with decreasing radius so that the acceleration of the water also becomes larger.

The curves of the equatorial diameter (maximum diameter) of the 2.7-mm-diam waterdrop at time intervals up to 200 μsec after the collision incident calculated by use of eq (31) for the three air-shock velocities for which experimental data were obtained are shown in figure 5 with the empirical curves. For the case that the Mach number of the shock was 1.3, the calculated curve lies above the empirical curve; for the case that the Mach number of the shock was 1.5, the calculated curve lies below the empirical curve; for the case that the Mach number of the shock was 1.7 the calculated curve lies very much below the empirical curve. In calculating points for the theoretical curves, the value of p_t, the stagnation pressure at the center of the windward face, was used for Δp. This is the very highest pressure that could be used for Δp. Actually, it may be a larger value than should be used and may account for the fact that the calculated curve for

the case that the Mach number of the shock was 1.3, the shape of which is closely similar to that of the empirical curve, lies above the empirical curve. However, if some fraction of p_t were used for Δp, the calculated curves for the cases that the Mach number of the shock was 1.5 and 1.7 would lie even further below the respective empirical curves. This observation leads to the thought that it may not be possible to explain the flattening of the waterdrop wholly in terms of the pressure difference which is set up between the poles and equator of the drop as a result of the airflow around it.

One possible explanation of the discrepancy may be that the waterdrop remembers the collision. If this is the case, the memory is a function of the air-shock velocity, and the memory is greater the higher the air-shock velocity is because the curves calculated by use of eq (31) have an increasingly poorer fit to the empirical curves for the case that the Mach number of the shock is 1.5 and 1.7, respectively. The memory may be a pressure pulse that is initiated in the water of the drop as the air shock passes and that subsequently undergoes successive reflection from the windward and leeward faces of the drop. As has been noted, because both faces of the waterdrop are free surfaces, this pulse will always reflect as a tension pulse from the leeward face and will always reflect as a pressure pulse from the windward face. In this way the value of Δp could become larger than p_t in air-shock-waterdrop collisions where a shock effect occurs.

There is another possible explanation. Attempts to calculate the acceleration of the 2.7-mm-diam waterdrop in the airflow behind shocks for which the Mach number is 1.5 (see section 4.7) indicate strongly that a central hole may form through the water disk to which the waterdrop flattens. The gradual development of this hole (see section 4.8) may account for an increase in the observed diameter of the water disk in excess of what can be accounted for by the pressure difference between the poles and equator of it alone.

4.7. Drift Velocity

Measurements of the distance from the edge of the fiducial marker to the leading edge of the waterdrop at various time intervals after the air-shock-waterdrop collision were made for three air-shock velocities. The fact that the waterdrops fell from the tip of the hypodermic needle with a slight scatter, and that the hypodermic needle itself was adjusted from time to time to insure that the waterdrops would fall through the hole in the floor of the shock tube, introduced a considerable amount of variation in the drift distances. It was arbitrarily decided that all negative values of drift should be recorded as zero drift and that wherever two consecutive spark pictures showed a zero or a negative value of drift all positive values for earlier periods of time should be disregarded. The measured distances of drift at various time intervals after the air-shock-waterdrop collision are plotted against the time elapsed since the collision in figures 6,A and 6,B for the case that the Mach number of the shock is 1.5 and 1.7, respectively. The slope of the drift-time curves of figures 6,A and 6,B were determined at 100-μsec intervals and these values, which are the drift velocities, are plotted against the time elapsed since the collision in figure 6,C. From figure 6,C it can be seen that the slope of the drift-velocity-against-time curve increases as the air-shock velocity increases. This is logical because the velocity of the airflow behind the shock is higher the higher the air-shock velocity.

From figure 6,C and table 1 it can be seen that 750 μsec after the air-shock-waterdrop collision, the drift velocity of the 2.7-mm-diam drop is about one-third of the airstream velocity for the case that the Mach number of the shock was 1.5. Reference to figure 10, picture 6, shows that at approximately this time after the air-shock-waterdrop collision the 2.7-mm-diam waterdrop was almost completely reduced to mist. Also, from figure 6,C and table 1 it can be seen that 600 μsec after the air-shock-waterdrop collision the drift velocity of the 2.7-mm-diam waterdrop is approximately one-half the airstream velocity for the case that the Mach number of the shock was 1.7. Reference to figure 12, picture 6, shows that 594 μsec after the air-shock-waterdrop collision the 2.7-mm-diam waterdrop is essentially a trail of mist. These observations show that the waterdrop does not acquire the airstream velocity before fragmentation is complete. This condition is more nearly realized when the Mach number of the shock is 1.7 than when it is 1.5. It may be found to be true for Mach numbers of the shock higher than 1.7. See section 4.4.b.

The slope of the curve of drift velocity plotted against the time elapsed since the air-shock-waterdrop collision is the acceleration given to the waterdrop. It is possible to calculate the acceleration for comparison with the observed slopes. In the case where there is relative accelerated motion between an object and a fluid there is an apparent change in the mass (M) of the object. The apparent addition to the mass (M) of the object is (M′) and in this paper is referred to as the additional mass. The force acting on the object is given by $(M+M')(dU/dt)$ where U is the relative motion between the object and the fluid. See reference [13]. The force on a water sphere that is moving in an infinite body of air is, assuming potential flow,

$$F=\frac{2}{3}\pi\rho_a r^3\alpha+\frac{4}{3}\pi r^3\rho_w\alpha, \tag{32}$$

where ρ_a, ρ_w are the densities of the airstream and of water, respectively, r is the radius of the sphere, and α is its acceleration. See reference [13]. The force can be evaluated from the distribution of pressure around a sphere in an airflow. Fage [4] has measured this pressure distribution for a 6-in.-diam sphere when the airflow velocity was 35 ft/sec. A graph of his measured values of the pressure on the sphere, p, above the free-stream pressure, p_2, is given in figure 14, B. The Reynolds number for his measurements was 110,000. Because the Reynolds numbers for the 2.7-mm-diam waterdrop in the flow

behind air shocks that had Mach numbers of 1.7, 1.5, and 1.3 were 89,000, 61,000, and 35,000, respectively, the pressure distribution around the waterdrop will be most nearly like that found by Fage [4] for the case that the Mach number of the shock was 1.7. However, the variation of the pressure distribution over this range of the Reynolds number should not be important. From the data of Fage [4], it appears that the minimum in the curve at 75° tends to be less marked as the Reynolds number is reduced. For the purpose of evaluating the acceleration of the waterdrop in the airflow behind a shock, it was assumed that the pressure follows the experimental curve of figure 14, B to 60°, that the minimum in the curve at 75° is absent, and that the pressure is constant over the remainder of the sphere from 60° to 180°. See appendix C. The total force on the sphere found by use of these assumptions is $0.244\ \pi r^2\rho_2 U_2^2$ where r is the radius of the sphere and ρ_2, U_2 are the density and the velocity of the airflow, respectively. Equating this to the force on a sphere in terms of its acceleration, α, given by eq (32) yields

$$\alpha=\frac{0.244\,U_2^2\rho_2}{\frac{2}{3}\rho_2 r+\frac{4}{3}\rho_w r}. \tag{33}$$

The velocity of the airflow behind the shock for the case that the Mach number of the shock is 1.5 is 2.37×10^4 cm/sec. Substituting the radius of the 2.7-mm-diam waterdrop for r, the acceleration α is found to be 1.64×10^6 cm/sec^2 in the airflow behind a shock that has a Mach number of 1.5. An enlarged graph of the waterdrop drift velocity after collision with a shock that has this Mach number is given in figure 15 for small values of time after the collision incident. At the end of 50 μsec after the air-shock-waterdrop collision, at which time the waterdrop is still close to its original spherical shape, the slope of the empirical drift velocity curve is 2×10^6 cm/sec^2.

A value of the acceleration similar to that obtained in the preceding calculation is found by equating the total force in terms of the acceleration as it is given in eq (32) to the drag resistance, $r^2\pi C_D\rho_2 U_2^2/2$ where C_D is the drag coefficient. From this equality,

$$\alpha=C_D U_2^2\rho_2 r^2/[\tfrac{4}{3}\rho_2 r^3+\tfrac{8}{3}\rho_w r^3]. \tag{34}$$

For a Reynolds number of 100,000, from the data of Wiesselsberger [18] and Allen [19], C_D for a sphere is 0.48. By use of this value of C_D, α is found to be 1.57×10^6 cm/sec^2 for the 2.7-mm-diam waterdrop in the airflow behind the shock for the case that the Mach number of the shock is 1.5. This is to be compared with the value of 1.64×10^6 cm/sec^2 obtained by the preceding calculation and with the observed value of 2×10^6 cm/sec^2.

When, however, an attempt is made to calculate the acceleration of the 2.7-mm-diam waterdrop in the airflow behind a shock that has a Mach number of 1.5 for times longer than 50 μsec after the air-shock-waterdrop collision, the result is found to be very different from the slope of the experimental drift

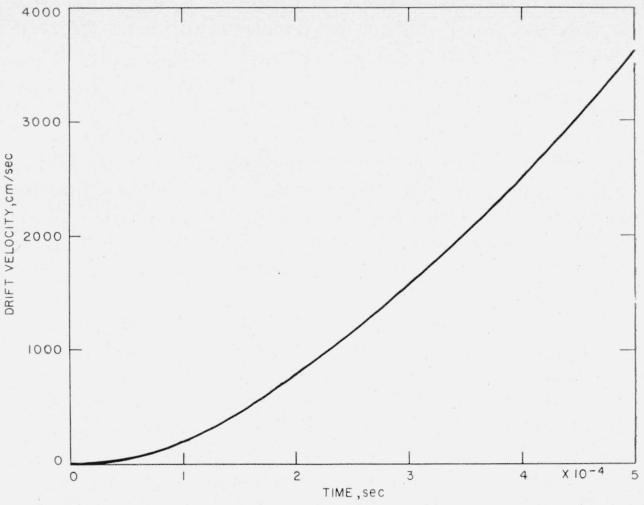

FIGURE 15. *Drift velocity of 2.7-mm-diam waterdrops in the airflow behind shocks for short times after the air-shock-waterdrop collision.*

Mach number of the air shock was 1.5. The slope of the curve at various times after the air-shock-waterdrop collision is as follows:

Time	Slope of curve
μsec	cm/sec^2
50	2×10^6
100	4
200	7.5
300	8.3
400	10

velocity curve shown in figure 15. The discrepancy appears to result from the fact that the waterdrop is changing shape. The calculated values of the acceleration should provide some additional evidence for the shape that the waterdrop assumes.

At the end of 94 μsec after the air-shock-waterdrop collison, for the case that the Mach number of the shock was 1.5, the waterdrop has already flattened in all directions perpendicular to the airflow (see fig. 9, picture 2) and at the end of 209 μsec after the collision incident it appears to have flattened into a water disk (see fig. 9, picture 3). The additional mass and the drag coefficient of a disk in an airflow are different from those of a sphere. If the waterdrop has become a water disk, its acceleration, α, should be given by

$$\alpha=\frac{C_D(U_2-W)^2\rho_2\pi r^2}{\frac{16}{3}\rho_2 r^3+\frac{8}{3}\pi\rho_w {r_o}^3} \tag{35}$$

where r is the radius of the water disk, r_o is the radius of the original water sphere, and W is the waterdrop drift velocity. The drag coefficient C_D for a disk is about unity and does not seem to change with change in the Reynolds number of the flow. Using values of W from the graph of figure 15 and values of r found from eq (31) (see fig. 5), the acceleration of the waterdrop under the assumption that it is a solid disk with a drag coefficient of unity was calculated by use of eq (35) for time intervals of 100, 200, and 300 μsec after the 2.7-mm-diam waterdrop collided with an air shock that had a Mach number

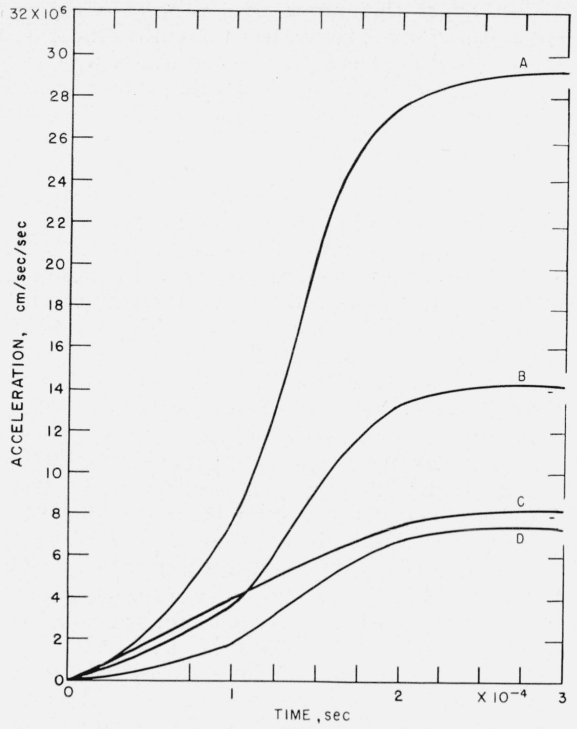

FIGURE 16. *Calculated acceleration of 2.7-mm-diam waterdrops in airflow behind shocks for three assumptions about the waterdrop shape.*

Mach number of the shock was 1.5. A, calculated with $C_D=1.0$ (solid disk); B, calculated with $C_D=0.48$ (solid sphere); C, observed; D, calculated with $C_{D,\,eff}=0.25$ (perforated disk).

of 1.5. The values of the acceleration obtained for this assumption in regard to the waterdrop comprise curve A of figure 16. Curve B of figure 16 is a graph of the values of the acceleration of the waterdrop obtained by use of eq (34) assuming that the waterdrop was a sphere of radius r as far as its drag coefficient ($C_D=0.48$), additional mass, and area presented to the flow are concerned, but a sphere of radius r_o as far as its real mass is concerned. It can be seen that the calculated acceleration-against-time curve, assuming that the waterdrop is a sphere, closely resembles the curve of the observed waterdrop acceleration up to 100 μsec after the air-shock-waterdrop collision but deviates sharply from the curve of the observed values of the acceleration for longer time intervals after the collision incident.

Inspection of eq (34) and (35) indicates that consideration of the loss from the original mass of the waterdrop in the form of mist will worsen rather than improve the agreement of the calculated with the observed values of the acceleration. It would appear that somewhere between 100 and 200 μsec after the air-shock-waterdrop collision the drag force is effectively reduced. Calculated values of the acceleration found with use of eq (35) and with an effective drag coefficient, $C_{D,\text{eff.}}$, arbitrarily taken to be one-fourth, were made and are plotted as curve D in figure 16. It can be seen that the values of the acceleration calculated with this arbitrary assumption about the drag coefficient are in fair agreement with the observed values of the acceleration for time intervals of 200 and 300 μsec after the collision incident but do not fit the experimental curve for smaller intervals of time after the collision incident. It can be deduced from the curves of figure 16 that a 2.7-mm-diam waterdrop remains essentially a sphere up to 100 μsec after collision with an air shock that has a Mach number of 1.5, but that somewhere between 100 and 200 μsec after the collision incident the drag force on it is materially reduced for some reason.

It is useless to look for an explanation of this behavior in the formation of a turbulent boundary layer. A turbulent boundary layer could logically be expected to form because of the irregularities that are observed on the windward face of the waterdrop, and a turbulent boundary layer does markedly reduce the drag coefficient of a sphere by causing the separation of the flow to move further back from the windward face. However, the waterdrop has flattened to a disk and the presence of a turbulent boundary layer does not affect the drag coefficient of a disk for which separation of the flow always occurs at the periphery. It would appear that the only explanation of the effective reduction of the drag force is the presence of a central hole or even of many holes in the disklike shape to which the waterdrop flattens. The presence of holes would reduce the area of the disk that is presented to the airflow and would therefore reduce the drag force.

To hypothesize that a central hole forms in the water disk to which the waterdrop flattens would relate the behavior of waterdrops in airstreams of very high velocity to what has been observed at lower velocities [15, 22]. See section 4.8. In view of the fact that the waterdrop probably does not enlarge by flattening into a solid disk, but that it is reduced to a water ring, the substantiation of Taylor's hypothesis of water loss by the stripping away of a surface layer which then breaks up to form mist (see section 4.4.b) should be reconsidered. An equation designed to trace the history of the waterdrop to the point of complete reduction to mist would have to take into account the loss of water from a moving water boundary layer during the successive stages when: (A) The original drop flattens to a disk and the moving boundary layer spills off the periphery of the water disk, (B) the water disk is perforated to form a water ring and the moving boundary layer spills off both the outer and inner periphery of the ring, and finally, (C) the ring of water eventually segments to form a chain of water beads and the moving boundary layer formed on the windward face of each of the beads spills off the periphery of the bead. After the water ring has segmented to form water beads, the total loss of water per unit time from moving windward-face boundary layers would be the sum of the losses per unit time from the aggregate of the individual small water spheres. In his equation to trace the history of the decay of the drop, Taylor [7] has only considered case (A).

The loss of water from a waterdrop that simply flattened into a coherent solid disk which did not develop holes can be found for various intervals of time after the air-shock-waterdrop collision from

Taylor's treatment. If x is taken to be the radius of the solid water disk, then eq (30) is simply

$$V=\left[4\pi\left(\frac{\rho_a}{\rho_w}\right)^{1/3}\left(\frac{\nu_a}{\nu_w}\right)^{1/6}\sqrt{\nu_w}\right]\int_o^t(U-W)^{1/2}r^{3/2}dt \quad (36)$$

$$V=0.241\int_o^t(U-W)^{1/2}r^{3/2}dt. \quad (37)$$

The lower portion of the drift velocity curve given in figure 15 is quite accurately represented by

$$W=kt^2 \quad (38)$$

where k is a constant which, from the empirical curve, has the value of 2×10^{10}. Using eq (31),

$$r=r_o+\frac{\Delta p}{3\rho_2 r_o}t^2 \quad (39)$$

where r is the radius of the water disk and r_o is the radius of the original undeformed water sphere. Substituting eq (38) and (39) into eq (37),

$$V=0.241\int[U-2\times10^{10}\,t^2]^{1/2}\left[r_o+\frac{\Delta p}{3\,\rho_2 r_o}t^2\right]^{3/2}dt. \quad (40)$$

The value of the right-hand side of eq (40) was found for t equal to 100, 200, and 300 μsec after the air-shock-waterdrop collision, respectively, for the case that the shock had a Mach number of 1.5. These values were plotted against the time and the area under the curve, that is, the total loss of volume of the drop, up to 100, 200, and 300 μsec after the collision incident or time zero was found to be 1.69×10^{-4}, 8.19×10^{-4}, and 18.89×10^{-4} cm^3, respectively.

The calculated acceleration at the end of 100 μsec after the air-shock-waterdrop collision, assuming that the waterdrop was still a sphere with $C_D=0.48$, was found to be 3.74×10^6 cm/sec^2 when no account was taken of the loss of mass by efflux and was found to be 3.83×10^6 cm/sec^2 when the loss of mass by efflux at the periphery was subtracted from the mass of the drop. The observed acceleration at the end of this time interval after the collision incident is 4.0×10^6 cm/sec^2. The acceleration was also calculated for the time intervals of 200 and 300 μsec after the air-shock-waterdrop collision. For these intervals of time after the collision incident, it was assumed that the waterdrop was a perforated disk with an effective drag coefficient $C_{D,\text{eff.}}=1/4$ to compensate for the loss of area and for the reduction of the actual drag coefficient and of the additional mass. The calculated acceleration for 200 μsec after the collision incident was found to be 6.94×10^6 cm/sec^2 when no account was taken of the loss of mass by efflux and was found to be 7.19×10^6 cm/sec^2 when the loss of mass by efflux was subtracted from the sum of the real mass and of the additional mass (of a solid disk). The observed acceleration at the end of this time interval after the collision incident is 7.5×10^6 cm/sec^2. The calculated acceleration for 300 μsec after the collision incident was found to be 7.34×10^6 cm/sec^2 when no account was taken of the loss of mass by efflux and was found to be 7.96×10^6 cm/sec^2 when the loss of mass by efflux was subtracted from the sum of the real mass and of the additional mass (of a solid disk). The observed acceleration 300 μsec after the collision incident is 8.3×10^6 cm/sec^2. A summary of the calculated values of the acceleration of a 2.7-mm-diam waterdrop in the airflow behind a shock that has a Mach number of 1.5 for various assumptions in regard to the shape of the drop is given in table 2.

It would appear that the loss of mass by efflux is too low at the end of 200 and of 300 μsec after the air-shock-waterdrop collision because larger values of this loss would improve the agreement between the calculated and observed acceleration for each of these time intervals. However, this is incorrect. For the case that the water disk is really a water ring having a width that would make the area of the ring equal to one-fourth the area of the disk,

$$\pi r^2-\pi R^2=0.25\pi r^2 \quad (41)$$

where r is the radius of the disk and R is the radius of the hole. Therefore, $R=\sqrt{3}\ r/2\sim0.87\ r$, and the width of the ring is 0.13 r. The volume loss with time for a solid water disk from eq (30) is

$$\frac{dV}{dt}=2\pi r\cdot\sqrt{x}\cdot K[f(t)] \quad (42)$$

where K is a constant, $f(t)$ is a function of the time,

TABLE 2. *Calculated acceleration for a 2.7-mm-diam waterdrop in the airflow behind a shock ($M_s=1.5$) with various assumption in regard to the shape assumed by the drop*

Drag coefficient, C_D	Acceleration, α		
	After 1×10^{-4} sec	After 2×10^{-4} sec	After 3×10^{-4} sec
	cm/sec^2	*cm/sec*^{2}	*cm/sec*^{2}
$C_D=0.48$, solid sphere	3.74×10^6	1.34×10^7	1.42×10^7
$C_D=1$, solid disk	7.78×10^6	2.78×10^7	2.93×10^7
$C_D=0.25$, perforated disk	1.94×10^6	6.94×10^6	7.34×10^6
$C_D=0.48$, solid sphere with Taylor loss	3.83×10^6		
$C_D=0.25$, perforated disk with Taylor loss		7.19×10^6	7.96×10^6
Observed acceleration	4.0×10^6	7.5×10^6	8.3×10^6

r is the radius of the solid water disk, and x is the distance that the wind blows over the water. Because the wind will blow from the stagnation point at the center of the disk to the periphery of the disk, the volume loss per unit time from the boundary layer that will form on the windward face of a solid water disk in an airflow is

$$\frac{dV}{dt}=2\pi r\cdot r^{1/2}\cdot K[f(t)]. \tag{43}$$

In the case of a water ring facing an airflow at 90° incidence, the stagnation point is a stagnation ring located at the center of the water ring. For the case that the water ring has one-fourth the area of a water disk of the same radius, the inner periphery is is $2\pi(0.87r)$, the outer periphery is $2\pi r$, and x is 0.13 $r/2$. Therefore, the volume loss with time for the water ring is

$$\frac{dV}{dt}=1.87(2\pi r)(0.25r^{1/2})K[f(t)]$$

$$\cong 0.5\{2\pi r\cdot r^{1/2}\cdot K[f(t)]\}. \tag{44}$$

Per unit time, the loss of mass by efflux from a ring that has one-fourth the area of a solid disk of the same radius is only half of that which would occur for the solid disk. The proper correction to bring the calculated values of the acceleration of the waterdrop at the time intervals of 200 and 300 μsec after the air-shock-waterdrop collision into agreement with the observed values should consist of a combination of reduction of the loss of mass by efflux, reduction of the real drag coefficient, and reduction of the additional mass.

4.8. Breakup of the Intact Portion of the Drop

Taylor [20] has shown theoretically that when two superposed fluids of different densities are accelerated in a direction perpendicular to their interface, this surface is unstable if the acceleration is directed from the lighter to the heavier fluid. Lewis [21] has shown experimentally that a layer of water driven by compressed air is unstable and that small disturbances, introduced into its surface against which the air is pressing to drive the liquid, grow so that it appears as though fingers of air move through the water layer. When these fingers reach the opposite surface of the water layer thin bubbles of water blow out ahead of them.

The acceleration of a waterdrop in the high-velocity airflow behind an air shock that has a Mach number of 1.5 is 4×10^6 cm/sec^2 100 μsec after the air-shock-waterdrop collision. Because this acceleration, which is very much greater than the acceleration of gravity, is perpendicular to the air-water interface, and because the acceleration is directed from the low-density air into the high-density water, the accelerating waterdrop is unstable.

Lane [22] and Hanson, Domich, and Adams [15] have observed that a waterdrop in a relatively low-velocity airstream first flattens in a direction perpendicular to that of the airflow and then develops a bubble. The bubble blows out downstream from the leeward face of the flattened waterdrop. In some cases the bubble that forms bursts and the remaining walls of it retract to the supporting ring of water that is left of the waterdrop. In other cases a head of water gathers at the center of the bubble and begins to move back toward and eventually through the water ring that is left of the drop, drawing the remaining walls of the bubble with it. Because bubble formation is in agreement with what Lewis [21] observed to happen in an unstable accelerating layer of liquid, this observation suggests the possibility that a dimple, formed at the stagnation point of the windward face of a waterdrop which is unstable because it is in a very rapid state of acceleration, may move through the drop like the fingers of air described by Lewis [21]. On reaching the leeward face of the waterdrop, it would blow a bubble precisely as the fingers of air observed by Lewis [21] blew out bubbles when they reached the leeward surface of the accelerating water layer. After the bubble burst, the waterdrop would have been reduced to a ring of water. Lewis [21] found that in the case where a layer of water was accelerated without first mechanically introducing surface irregularities on it, the slight surface tension curvature at the sides of the channel he used and other unavoidable sources of small disturbances are sufficient to start the instability. In this case, however, there is a time lag before an appreciable top surface amplitude occurs.

In the present investigation, no evidence of bubble formation was seen in any of the spark pictures that were taken of fragmenting waterdrops in the high-velocity airflows behind air shocks that had Mach numbers of 1.3, 1.5, and 1.7. However, the time interval between spark pictures was not made very small so that it is possible that, if bubble formation occurs very rapidly in these high-velocity airstreams, it could have been missed.

Lewis [21] found that the velocity of penetration of an air finger was given by the expression

$$v_p=C_1[(g_1-g)r_1]^{1/2} \tag{45}$$

where C_1 is a constant which for water has the value of 1.11, g_1 is the acceleration of the water layer, g is the acceleration of gravity, and r_1 is the radius of curvature of the air finger. He states that this equation, with $C_1=1.11$, overestimates the value of the velocity when r_1 is small (~0.25 in.) and underestimates the value of the velocity when r_1 is large (~0.9 in.).

From the requirement that an effective drag coefficient of one-fourth is needed to obtain agreement between calculated and observed acceleration of the waterdrop at the end of the interval of 200 μsec after the air-shock-waterdrop collision, it would seem that the bubble has formed and burst by this time if the process of bubble formation actually occurs. From eq(45) it is possible to estimate very roughly the

time that would be required for an air finger, which may form at the stagnation point of the windward face, to pass through the thickness of the drop. The average value of the acceleration of the waterdrop in the airflow behind a shock that has a Mach number of 1.5 over the first 200 μsec after the air-shock-waterdrop collision is 3.8×10^6 cm/sec^2. The original radius of the waterdrop was 0.14 cm and it can be assumed that the radius of the air finger is about half of this. If these values are substituted into eq(45), the velocity of penetration is found to be 580 cm/sec. From figure 9, picture 2, the thickness of the flattening waterdrop at close to 100 μsec after the air-shock-waterdrop collision is 0.208 cm so that the time required for penetration would be about 360 μsec. This is of the right order of magnitude but is too large because the requirement of an effective drag coefficient of one-fourth is needed to obtain agreement between the calculated and observed value of the acceleration, which was taken to be evidence that a hole has formed in the water disk, 200 μsec after the collision. However, the roughness of the assumption that the radius of curvature of the air finger is about half the radius of the original waterdrop could account for the discrepancy.

If a water ring forms, its diameter should remain constant because the water ring is subject to the check of surface tension and because there is no longer a pressure difference acting between the centers of the faces and the periphery of the water ring that would tend to drive it to larger size. This constant diameter is precisely what is observed in the plateau region in the time interval that extends from about 220 μsec to about 300 μsec in the curves of figure 5. In the pictures obtained by Hanson, Domich, and Adams [15] of the fragmentation of waterdrops in lower velocity airflows, it can be seen that the water ring itself eventually segments into a chain of water beads. It can be assumed that this breakup of the water ring has occurred at the end of the plateau region in the curves of figure 5, that is, 300 μsec after the air-shock-waterdrop collision, because after this there is a further increase of the apparent diameter of the waterdrop perpendicular to the direction of the airflow. This further increase in the diameter of the structure that remains of the waterdrop could be accounted for as a drifting apart of the water beads into which the ring of water that remains of the drop has broken.

For the case of shocks having Mach numbers of 1.3 and 1.5, for which sufficient data exist to identify the plateau region, the formation of the plateau seems to occur in about the same time interval, namely, from about 220 to about 300 μsec after the air-shock-waterdrop collision. It seems reasonable to think that the plateau should be displaced to lower values of the time as the air-shock velocity is increased because the acceleration of the waterdrop is higher as the velocity of the airflow about it is higher, and the time required to pierce the waterdrop with an air finger to form a water ring is proportional to its acceleration. More data than those presented here are needed. It will require taking pictues of fragmenting waterdrops with the camera arranged to look down the length of the shock tube rather than to look through it from the side to determine what actually does occur.

The importance of knowing that segmentation of the water ring occurs at the end of 300 μsec after the air-shock-waterdrop collision and of knowing whether or not it occurs sooner as the shock velocity is increased is the bearing that this information has on the high-speed-rain-erosion problem. Segmentation of the ring of water that remains of the original waterdrop into small water beads would represent a large reduction of its ability to produce erosion damage on striking a solid surface.

It is noteworthy that the small waterdrop started to drift sooner than the large waterdrop. From inspection of either eq (33) or of eq (34), it can be seen that a small waterdrop has a greater acceleration than a large waterdrop in airstreams of the same velocity. It is evident from eq (45), therefore, that the small waterdrop will be pierced to form a water ring sooner than a large waterdrop will. The 1.4-mm-diam waterdrop should be expected, therefore, to become unstable and to undergo ring formation and segmentation before the 2.7-mm-diam waterdrop does.

4.9. Limitations of the Observations

It is noteworthy that Hanson, Domich, and Adams [15], using a 0.3-mm-diam drop of methyl alcohol and an airflow having a velocity of 0.695×10^4 cm/sec, found that the drop of alcohol had reacted to the airflow in a marked way at the end of only 10 μsec; the drop of alcohol was flattened against the wind, streamers of *liquid* were pouring off the periphery of it, and a pointed structure that was oriented in the direction from which the wind was coming had developed in the center of the windward face of it. This evidence indicates that the fragmentation mechanism is dependent on the drop diameter, the velocity of the airflow, and the density, surface tension, and viscosity of the liquid of the drop. The results that were obtained and the conclusions that have been drawn in the study that is reported here apply only to drops of water that have a diameter in the range of 1.4 to 2.7 mm and that disintegrate in airstreams, the velocities of which are in the range of 1.52×10^4 to 3.16×10^4 cm/sec. To extrapolate the conclusions to the fragmentation of liquid drops under conditions for which the values of the variables are outside the range for which the observations of this study were made may result in spurious inferences because it appears that not only the rate of the fragmentation but also the very mechanism by which it occurs is strongly dependent on these variables. The mechanism by which the fragmentation occurs for various sized drops of liquids of different properties in airstreams of different velocities has many aspects of basic interest. Much more experimental work will be required to show the correct interdependence of the variables that are involved.

5. Importance of the Fragmentation Time of Waterdrops to the Problem of Collision With Rain of Objects Moving at Supersonic Velocities

A blunt object moving through air at supersonic velocity is accompanied by a shock wave that is separated from the leading surface of the object by a zone in which air is moving at high velocity ahead of the object. The width of the zone of separation between the shock wave and the leading surface of the object that is producing it depends on the radius of curvature of the object and on the velocity at which it is moving. It was pointed out earlier that the existence of this phenomenon might prove to be of considerable importance to the high-speed rain-erosion problem for objects moving at supersonic velocities. If a waterdrop would be shattered under the conditions that exist in the zone by which a shock is separated from the leading surface of the object that is producing it, and if this fragmentation of the waterdrop would have time to occur before the surface of the object collided with the waterdrop, the erosion problem might be much less serious at supersonic velocities than at subsonic velocities. It seemed possible that it might be bypassed entirely. It was to determine whether or not such an escape from the problem of rain erosion exists at supersonic velocities that the present investigation of the time required for the fragmentation of waterdrops was undertaken.

The distance by which the detached shock, formed in front of a sphere that is moving at supersonic velocity, is separated from the sphere that is producing it, is plotted against the Mach number at which the sphere is moving for four sphere diameters in figure 17. The time required to traverse, at the sphere velocity itself, the distance by which the shock is separated from the sphere is plotted against the Mach number at which the sphere is moving for four sphere diameters in figure 18. The velocity of the sphere is the same as the velocity of the shock. The data used to produce these curves are those of Heybey [23] for shocks having Mach numbers of 2 and 3 and those given by Shapiro [24] for shocks having Mach numbers less than 2. See table 3.

TABLE 3. *Shock-detachment distance, d_s, for various shock velocities*

Shock velocity	d_s/sphere radius [a]
1.15 Mach	1.48
1.3	1.0
1.36	.84
1.62	.54
1.8	.40
2.0	.31
3.0	.20

[a] See references [23, 24].

If a sphere moving at a Mach number of 1.3 were to encounter rain, the detached shock preceding it, and the zone of separation between this shock and the sphere, would run over the raindrops. From the graph of figure 18, the time that the raindrops would have to become completely fragmented so as not to damage the sphere at all on colliding with the leading surface of it is 345 μsec if the sphere diameter is 1 ft, 670 μsec if the sphere diameter is 2 ft, and 1,025 μsec if the sphere diameter is 3 ft. The stage of

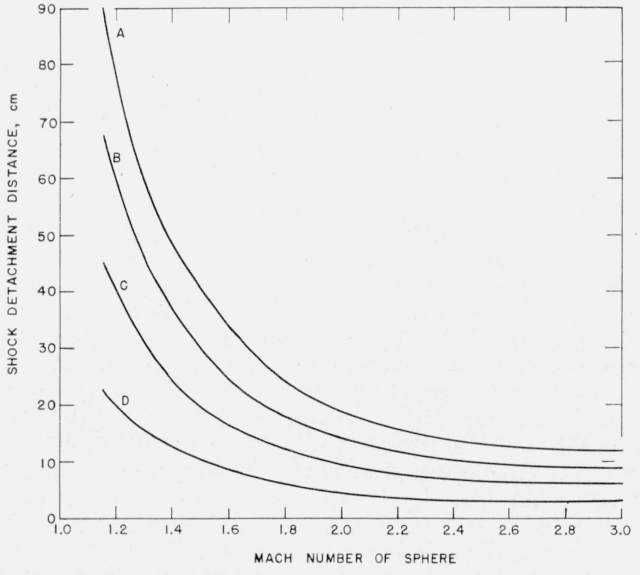

FIGURE 17. *Shock detachment distance for spheres.*

A, 4-ft-diam sphere; B, 3-ft-diam sphere; C, 2-ft-diam sphere; D, 1-ft-diam sphere.

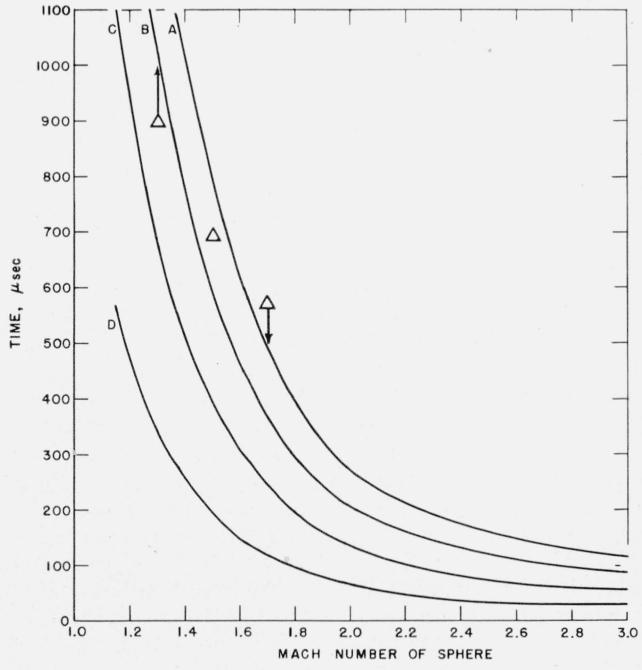

FIGURE 18. *Time during which fragmentation must occur to prevent a waterdrop-sphere collision.*

A, 4-ft-diam sphere; B, 3-ft-diam sphere; C, 2-ft-diam sphere; D, 1-ft-diam sphere. Observed time required to reduce a small waterdrop to a trace of mist is indicated with triangular points.

disintegration that a 2.7-mm-diam waterdrop would have reached at the end of the protection time afforded by a 1-ft-diam sphere moving at a Mach number of 1.3 is between that shown in pictures 2 and 3 of figure 4. The stage of disintegration that a 2.7-mm-diam waterdrop would have reached at the end of the protection time afforded by a 2-ft-diam sphere moving at a Mach number of 1.3 is between that shown in pictures 5 and 6 of figure 4. That is, the waterdrop residues shown in figure 4, pictures 2 and 3, and those shown in figure 4, pictures 5 and 6, are about representative of the waterdrop fragments that would strike the leading surface of a 1-ft-, and of a 2-ft-diam sphere that was moving at a Mach number of 1.3, respectively. It can be seen that the waterdrop is not reduced completely to a trace of mist at the end of the allowed times when the Mach number of the shock is 1.3. However, from a comparison of the degree of fragmentation of 1.4-mm-diam waterdrops, it appears that this condition may be realized within the protection time afforded by a 4-ft-diam sphere, which on extrapolation of curve A of figure 18, might be as much as 1,200 μsec.

Similarly, if the Mach number of the sphere were 1.5 when it intercepted rain, the time interval in which the raindrops must fragment if they are not to damage the leading surface of the sphere when they collide with it is 200 μsec for a 1-ft-diam sphere, 390 μsec for a 2-ft-diam sphere, 600 μsec for a 3-ft-diam sphere, and 780 μsec for a 4-ft-diam sphere. By inspection of figures 10 and 11 it can be seen that both 3-ft- and 4-ft-diam spheres would be completely protected from 1.4-mm-diam waterdrops and that the 4-ft-diam sphere would be fairly well protected against 2.7-mm-diam waterdrops.

Finally, if the sphere were moving at a Mach number of 1.7 when it intercepted rain, the time interval in which the waterdrops must disintegrate if they are not to damage the leading surface of the sphere when they collide with it is 120 μsec for a 1-ft-diam sphere, 245 μsec for a 2-ft-diam sphere, 365 μsec for a 3-ft-diam sphere, and 495 μsec for a 4-ft-diam sphere. From the appearance of waterdrop residues seen in spark pictures when the Mach number of the shock was 1.7, it seems probable that a 4-ft-diam sphere would be completely protected from 1.4-mm-diam waterdrops and that it may be fairly well protected from 2.7-mm-diam waterdrops. See figure 12.

The sphere diameters required in order to provide sufficiently long protection times to reduce 1.4-mm-diam and 2.7-mm-diam waterdrops to mist are listed in table 4 for the case that the sphere is moving at a Mach number of 1.3, 1.5, and 1.7. How much damage will be done by the impingement of waterdrop fragments on spheres having diameters smaller than the minimum required for complete protection can only be a matter for conjecture until an actual test is made. Certainly, the damage will be found to be very much less severe than would be expected if the entire waterdrop should impinge as a spherical projectile at these velocities.

TABLE 4. *Sphere diameters that will afford sufficiently long protection time to reduce waterdrops of two sizes to mist*

Velocity of shock or of sphere	Minimum sphere diameter required so that water mist only will impinge on the leading surface of the sphere
	ft
M_s=1.3	
1.4-mm waterdrop diameter	4
2.7-mm waterdrop diameter	>>4
M_s=1.5	
1.4-mm waterdrop diameter	3
2.7-mm waterdrop diameter	≳4
M_s=1.7	
1.4-mm waterdrop diameter	4
2.7-mm waterdrop diameter	≳4

It is important to know whether the degree of fragmentation reached at the end of the protection time afforded by any sphere diameter is greater or less as the velocity of the shock is increased. For the case of the 1-ft-diam sphere it is a question of evaluating the degree of waterdrop fragmentation 345 μsec after collision with a shock moving at a Mach number of 1.3 (fig. 4), 200 μsec after collision with a shock having a Mach number of 1.5 (fig. 10), and 120 μsec after collision with a shock moving at a Mach number of 1.7 (fig. 12). For the case of the 2-ft-diam sphere it is a question of comparing the extent of waterdrop fragmentation 670 μsec after collision with a shock moving at a Mach number of 1.3, 390 μsec after collision with a shock moving at a Mach number of 1.5, and 245 μsec after collision with a shock moving at a Mach number of 1.7. For the case of the 3-ft-diam sphere, comparison must be made of the observed fragmentation 1,025 μsec after collision with a shock moving at a Mach number of 1.3, 600 μsec after collision with a shock moving at a Mach number of 1.5, and 365 μsec after collision with a shock moving at a Mach number of 1.7. From a comparison of the degree of fragmentation observed at approximately the end of the allowed protection time for three sphere diameters at each of the three air shock velocities, it appears that the degree of fragmentation of waterdrops that exist within the zone of detachment within the protection time afforded by a detached shock will be found to be either about comparable for shocks of different velocities or may be somewhat greater the higher the velocity of the shock.

Finally, it may be asked whether there is a basis for assuming that at some much higher velocity than any used in this investigation the waterdrop will be completely reduced to a trace of mist within the protection time available for 1-ft- or 2-ft-diam spheres before the residue of the drop will strike the leading surface of the sphere at that velocity. The data at hand are not sufficient to answer this question. It is not even known that it is necessary to reduce the waterdrop completely to mist before the damage done by it on impingement will be negligible. A rough answer can be attempted on the assumption that complete reduction to mist is necessary. Because only the 1.4-mm-diam waterdrops were completely reduced to mist after collision with shocks

moving with Mach numbers of 1.3, 1.5, and 1.7 within the time intervals that were investigated, an answer can only be attempted for waterdrops of this size. The approximate time required to reduce a 1.4-mm-diam waterdrop to a trail of mist is plotted in figure 18 against the Mach number of the shock with which it collided. The arrow drawn down from the time required when the shock had a Mach number of 1.7 indicates that it may be lower than 574 μsec. The arrow drawn upward from the point on the graph for the time required when the shock had a Mach number of 1.3 indicates that the time actually required to reduce a 1.4-mm-diam waterdrop to mist is greater than 901 μsec. The fewness of the points and the ambiguity in them leave unanswered the question as to whether at some high Mach number of the shock the curve on which these three points lie will ever intersect and drop below curve C or curve D of figure 18. It is conceivable that at a Mach number of the shock greater than 3 this condition may be realized, but further observations at Mach numbers of the shock higher than 1.7 will be needed to justify such an extrapolation.

Even if it is found that there is no high Mach number of the shock at which 1.4-mm-diam waterdrops are completely reduced to mist before they impinge against spheres of small diameters, there is another means which may be used to accomplish this. By proper design, the detached shock wave produced by a blunt object moving through air at supersonic velocity can be pushed out to increase the detachment distance and hence to increase the time during which fragmentation of waterdrops may occur before they impinge against the leading surface of the object. Construction of a retractable cowl around a sphere, for example, would have this effect, and the increased aerodynamic drag need only be a disadvantage during actual flight through rain. It appears that recourse to such a device will bypass the high-speed rain-erosion problem completely at supersonic velocities. Use of such a device to insure complete immunity from rain-erosion damage at supersonic velocities could only be justified, however, if the aerodynamic disadvantage is preferable to the impaired performance of pointed radomes which are only slightly vulnerable to rain erosion attack.

The author thanks J. M. Burgers, Z. I. Slawsky, W. H. Heybey, Edward F. Smiley, Adolf H. Lange, Chan Mou Tchen, and John Mandel for contributions to theoretical aspects of the problem and Ben Crapo, Harriet A. Baker, and Robert R. Pizer for assistance with the optics, electronics, and photography.

6. Appendix A. Loss of Water Per Unit Time From the Moving Boundary Layer [6]

Consider that air (sub-a notation) in the airflow behind an air shock is moving at velocity U_2 over the water (sub-w notation) of the windward face of a waterdrop. A boundary layer is set up in the water and in the air on either side of the interface. The velocity in the boundary layer is u. In the water boundary layer, $u=u_wU_2$; in the air boundary layer, $u=u_aU_2$; u_w and u_a are dimensionless coefficients. At the interface, $u_w=u_a$; at some depth below the surface, $u_w=0$; at some height above the air-water interface, $u_a=1$. If the x-axis lies in the air-water interface of the windward face of the waterdrop, and the y-axis, perpendicular to it, is positive both upstream in the air and downstream in the water, the boundary layer velocities may be expressed as

$$u_a=u/U_2=1-Ae^{-y/(\alpha_a\sqrt{x})}$$

$$u_w=u/U_2=(1-A)e^{-y/(\alpha_w\sqrt{x})}$$

where A, α_a, and α_w are quantities that must be determined. This choice satisfies the boundary conditions that as $y\to\infty$, $u_a\to1$, and $u_w\to0$, and that for $y=0$, $u_a=u_w$. This choice also satisfies Karman's boundary layer momentum equations. The Karman equation for air is

$$\frac{d}{dx}\int_0^\infty u(U_2-u)dy=-\nu_a\left[\frac{\partial u}{\partial y}\right]_{y=0} \tag{A1}$$

where ν is the kinematic viscosity.

Dividing both sides by U_2^2 gives the form

$$\frac{d}{dx}\int_0^\infty \frac{u}{U_2}\left[1-\frac{u}{U_2}\right]dy=-\frac{\nu_a}{U_2}\left[\frac{\partial(u/U_2)}{\partial y}\right]_{y=0}. \tag{A2}$$

or

$$\frac{d}{dx}\int_0^\infty\left[Ae^{\frac{-y}{\alpha_a\sqrt{x}}}-A^2e^{\frac{-2y}{\alpha_a\sqrt{x}}}\right]dy=-\frac{\nu_a}{U_2}\left[\frac{\partial}{\partial y}\left(1-Ae^{\frac{-y}{\alpha_a\sqrt{x}}}\right)\right]_{y=0}. \tag{A3}$$

Performance of the indicated operations produces the result

$$\alpha_a{}^2=\frac{2\nu_a}{U_2\left[1-\frac{A}{2}\right]}. \tag{A4}$$

The Karman equation for the water is

$$\frac{d}{dx}\int_0^\infty u^2\,dy=-\nu_w\left[\frac{\partial u}{\partial y}\right]_{y=0}. \tag{A5}$$

Dividing through by $U_2{}^2$ gives the form

$$\frac{d}{dx}\int_0^\infty (u/U_2)^2\,dy=-\frac{\nu_w}{U_2}\left[\frac{\partial}{\partial y}(u/U_2)\right]_{y=0}, \tag{A6}$$

or

$$\frac{d}{dx}\int_0^\infty (1-A)^2e^{\frac{-2y}{\alpha_w\sqrt{x}}}dy=-\frac{\nu_w}{U_2}\left[\frac{\partial}{\partial y}(1-A)\,e^{\frac{-y}{\alpha_w\sqrt{x}}}\right]_{y=0}. \tag{A7}$$

[6] With minor changes, the treatment presented here is that given by Taylor in reference [7].

Performance of the indicated operations produces the result

$$\alpha_w^2=\frac{4}{U_2}\frac{\nu_w}{(1-A)}. \tag{A8}$$

The condition of continuity of tangential stress, F, imposes the condition that

$$\begin{aligned}\frac{F}{U_2}&=\rho_a\nu_a\left[\frac{\partial}{\partial y}\left(\frac{u}{U_2}\right)\right]_{y=0}=-\rho_w\nu_w\left[\frac{\partial}{\partial y}\left(\frac{u}{U_2}\right)\right]_{y=0}\\&=\rho_a\nu_a\left[\frac{\partial}{\partial y}\left\{1-Ae^{\frac{-y}{\alpha_a\sqrt{x}}}\right\}\right]_{y=0}\\&=-\rho_w\nu_w\left[\frac{\partial}{\partial y}\left\{(1-A)\,e^{\frac{-y}{\alpha_w\sqrt{x}}}\right\}\right]_{y=0}\\&=\rho_a\nu_a\left[\frac{A}{\alpha_a\sqrt{x}}\right]=\rho_w\nu_w\left[\frac{(1-A)}{\alpha_w\sqrt{x}}\right].\end{aligned} \tag{A9}$$

From eq (A8),

$$A=1-[4\nu_w/(\alpha_w^2U_2)], \tag{A10}$$

and by substitution of the expression for $(1-A)$ in eq (A9)

$$\frac{F\sqrt{x}}{U_2}=\frac{\rho_w\nu_w}{\alpha_w}\left[\frac{4\nu_w}{\alpha_w^2U_2}\right]. \tag{A11}$$

Similarly from eq (A4)

$$A=2-[4\nu_a/(\alpha_a^2U_2)] \tag{A12}$$

and by substituting eq (A12) into eq (A9)

$$\frac{F\sqrt{x}}{U_2}=\frac{\rho_a\nu_a}{\alpha_a}\left[2-\frac{4\nu_a}{\alpha_a^2U_2}\right]. \tag{A13}$$

Equating the expression for A given by eq (A10) and (A12)

$$\frac{4\nu_w}{\alpha_w^2U_2}=\frac{4\nu_a}{\alpha_a^2U_2}-1 \tag{A14}$$

and by equating the expressions for $F\sqrt{x}/U_2$ given by eq (A11) and (A13)

$$\frac{\rho_w\nu_w}{\alpha_w}\left[\frac{4\nu_w}{\alpha_w^2U_2}\right]=\frac{\rho_a\nu_a}{\alpha_a}\left[2-\frac{4\nu_a}{\alpha_a^2U_2}\right]. \tag{A15}$$

From eq (A14) and (A15) by use of the condition that when $\nu_w/(\alpha_w^2U_2)$ is small, $\nu_a/(\alpha_a^2U_2)\cong 1/4$, it can be shown that

$$\frac{\nu_w}{\alpha_w^2U_2}\cong\frac{1}{4}\left(\frac{\rho_a}{\rho_w}\right)^{2/3}\left(\frac{\nu_a}{\nu_w}\right)^{1/3}. \tag{A16}$$

Substituting the values of ρ_a, ν_a for the airstream flowing behind an air shock that has a Mach number of 1.5 (see table 1) and the values of $\rho_w=0.998$, $\nu_w=0.01$, produces the result that $\nu_w/(\alpha_w^2U_2)\cong 0.009187$, from which $\alpha_w=10.43\ (\nu_w/U_2)^{1/2}$. From eq (A14) and the value of $\nu_w/(\alpha_w^2U_2)$, it is found that $\nu_a/(\alpha_a^2U_2)=0.2592$, and $\alpha_a=1.964\ (\nu_a/U_2)^{1/2}$. Using these expressions for α_a and α_w, values of the dimensionless quotient of the boundary layer velocity divided by the free-stream velocity, u/U_2, were calculated from the exponential expressions for u_a and u_w that were chosen initially. The kinematic viscosity of the airflow behind an air shock that has a Mach number of 1.5 was used for ν_a in the expression for α_a. The calculated values of u/U_2 are plotted in figure 19.

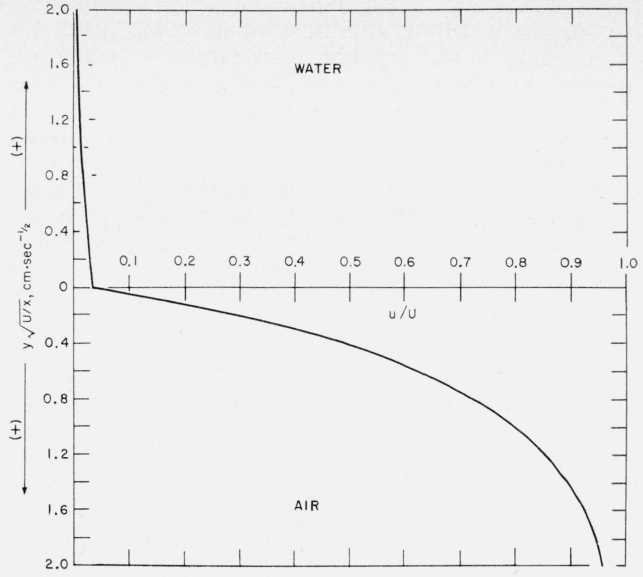

FIGURE 19. *Boundary layers in air and water under the conditions that exist in the airstream flowing behind a shock.*

Mach number of the air shock is 1.5.

The efflux of water out of the boundary layer per unit length of periphery when the mass of water itself has velocity W is

$$\int_0^\infty (U_2-W)(1-A)e^{\frac{-y}{\alpha_w\sqrt{x}}}dy=(U_2-W)(1-A)\alpha_w\sqrt{x}. \tag{A17}$$

By use of eq (A10) and of eq (A16) and by multiplying by the periphery, $2\pi r$, the total efflux or total loss of volume per unit time is

$$\frac{dV}{dt}=4\pi r\left(\frac{\rho_a}{\rho_w}\right)^{1/3}\left(\frac{\nu_a}{\nu_w}\right)^{1/6}\sqrt{U_2-W}\sqrt{\nu_w}\sqrt{x}. \tag{A18}$$

7. Appendix B. Flattening of the Waterdrop With Time

The sphere of liquid is located at the origin of a rectangular coordinate system in which the x-axis runs parallel to the direction of the airflow in the shock tube. The stagnation pressure exists at $x=\pm r$ where r is the radius of the liquid sphere. It

[7] This solution of the time dependence of the flattening of a waterdrop in an air flow was developed by J. M. Burgers.

is assumed that the liquid in the sphere is incompressible and that motion throughout the whole volume of the sphere as a result of the pressure distribution begins instantaneously.

The continuity equation is

$$\frac{\partial u}{\partial x}+\frac{\partial v}{\partial y}+\frac{\partial w}{\partial z}=0, \tag{B1}$$

where u, v, w are the velocities along the x-, y-, and z-axis, respectively. To satisfy the continuity equation

$$u=-2bx,\ v=by,\ w=bz, \tag{B2}$$

where b is a function of the time that must be determined. Also, because

$$u=-\frac{\partial \phi}{\partial x},\ v=-\frac{\partial \phi}{\partial y},\ w=-\frac{\partial \phi}{\partial z}, \tag{B3}$$

where ϕ is the velocity potential, it follows that [8]

$$\phi=b\left[-x^2+\frac{1}{2}y^2+\frac{1}{2}z^2\right]. \tag{B4}$$

The equation of motion is

$$p=-\rho\frac{\partial \phi}{\partial t}+\text{constant} \tag{B5}$$

where ρ is the density of the liquid and t is the time. The term $\frac{1}{2}\rho\ (u^2+v^2+w^2)$ is neglected as small for short times after the air-shock-waterdrop collision. Applying the equation of motion at the points $x=\pm r$ on the surface of the sphere

$$p_x=\rho r^2\frac{db}{dt}+\text{constant} \tag{B6}$$

and applying the equation at the points $y=\pm r$, $z=\pm r$ on the surface of the sphere

$$p_{y,z}=-\frac{1}{2}\rho r^2\frac{db}{dt}+\text{constant}. \tag{B7}$$

The pressure difference is

$$\Delta p=p_x-p_{y,z}=\frac{3}{2}\rho r^2\frac{db}{dt} \tag{B8}$$

and therefore

$$\frac{db}{dt}=\frac{2}{3}\frac{\Delta p}{\rho r^2}. \tag{B9}$$

If the pressure difference is independent of the time,

$$b=\frac{2}{3}\frac{\Delta p}{\rho r^2}t. \tag{B10}$$

The outward velocity of liquid at the equator of the sphere is given by $v=by$, $w=bz$ from eq (B2), and at the points where $y=\pm r$, $z=\pm r$,

$$v=w=\frac{2}{3}\frac{\Delta p}{\rho r}t. \tag{B11}$$

The outward displacement d at the points $y=\pm r$, $z=\pm r$ is

$$d=\frac{2}{3}\frac{\Delta p}{\rho r}\int_0^t t\,dt$$

$$=\frac{1}{3}\frac{\Delta p}{\rho r}t^2. \tag{B12}$$

The increase in the diameter of the waterdrop perpendicular to the direction of the airflow is 2 d.

8. Appendix C. Total Force Acting on the Waterdrop

Consider the differential area to be a narrow band around the sphere. See inset, figure 14, A. The width of the differential area is the arc subtended by the angle $d\theta$ and is $rd\theta$ where r is the radius of the sphere. The radius of the band of differential area is $r\sin\theta$, the circumference of the band is $2\pi r\sin\theta$, and the area of the band is $2\pi r^2\sin\theta\,\mathrm{d}\,\theta$. Because the pressure curve of figure 14, B is quite accurately given by $\frac{1}{2}\rho_2 U_2^2(1-2\sin^2\theta)$ up to 60°, the horizontal component of the force on the differential area at any angle θ is $\frac{1}{2}\rho_2 U_2^2\ (1-2\sin^2\theta)\ (\cos\theta)$, and the differential force, dF_θ, is

$$dF_\theta=\frac{1}{2}\rho_2 U_2^2\,(1-2\sin^2\theta)\,(\cos\theta)\,(2\pi r^2\sin\theta d\theta). \tag{C1}$$

Hence, the force, F_θ, is

$$\overset{\theta=\pi/3}{\underset{\theta=0}{F}}=\pi r^2\rho_2 U_2^2\left[\int_0^{\pi/3}\sin\theta\cos\theta d\theta-2\int_0^{\pi/3}\sin^3\theta\cos\theta d\theta\right], \tag{C2}$$

$$\overset{\theta=\pi/3}{\underset{\theta=0}{F}}=\pi r^2\rho_2 U_2^2\left|\frac{\sin^2\theta}{2}-\frac{2\sin^4\theta}{4}\right|_0^{\pi/3}, \tag{C3}$$

$$=0.094\,\pi r^2\rho_2 U_2^2. \tag{C4}$$

The horizontal component of the force on the differential element in the region $\pi/3\leq\theta\leq\pi$ is given by $-0.4(\frac{1}{2}\rho_2 U_2^2)\cos\theta$, so the force on this part of the sphere is given by

$$\overset{\theta=\pi}{\underset{\theta=\pi/3}{F}}=-0.4\left(\frac{1}{2}\rho_2 U_2^2\right)\int_{\pi/3}^{\pi}2\pi r^2\sin\theta\cos\theta d\theta \tag{C5}$$

$$=-0.4\,\pi r^2\rho_2 U_2^2\left|\frac{\sin^2\theta}{2}\right|_{\pi/3}^{\pi} \tag{C6}$$

$$=0.15\,\pi r^2\rho_2 U_2^2. \tag{C7}$$

Therefore, the total force on the sphere is $0.244\ \pi r^2\rho_2 U_2^2$.

[8] The solution given is not unique but consideration of the general case shows that an equation of the form of eq (B9) should be found except that the dimensionless coefficient 2/3 may be different.

9. References

[1] Edward F. Smiley and Ernst H. Winkler, J. Chem. Phys. **22,** 2018 (1954).
[2] Ames Research Staff, NACA Report 1135 (1953).
[3] J. M. Burgers, Ned. Akad. v. Wetensch. Afd. Natuurkunde, LII, No. 8 en 9 (1943).
[4] A. Fage, Aeronautical Research Committee Reports and Memoranda, R and M No. 1766, ARC Technical Report (1937).
[5] John W. Strutt, Baron Rayleigh, Theory of sound (Dover Publications, New York, N. Y., 1945).
[6] P. Lenard, Ann. phys. **266,** 209, Neue Folge Band XXX (1887).
[7] Sir Geoffrey Taylor, Porton Paper 6600/5278/49.
[8] Robert H. Cole, Underwater explosions (Princeton Univ. Press, Princeton, N. J., 1948).
[9] Robert Williams Wood, Supersonics (Brown Univ., Providence, R. I., 1939).
[10] John S. Rhinehart, J. Appl. Phys. **22,** 555 (1951).
[11] John S. Rhinehart, NOTS TM No. 348 (May 1952).
[12] Joseph B. Keller and Ignace Kolodner, J. Appl. Phys. **25,** 918 (1954).
[13] Sir Horace Lamb, Hydrodynamics, 6th ed. (Cambridge Univ. Press, New York, N. Y., 1932).
[14] W. R. Lane and H. L. Green, The mechanics of drops and bubbles in Surveys of mechanics, edited by G. K. Batchelor and R. M. Davies (Cambridge Univ. Press, New York, N. Y., 1956).
[15] A. R. Hanson, E. G. Domich, and H. S. Adams, Research Report No. 125, Univ. Minn. Inst. Technol., Dept. of Aeronaut. Eng., Rosemount Aeronaut. Labs., Minneapolis, Minn. (January 1956).
[16] C. M. Tchen, J. Appl. Phys. **27,** 1533 (1956).
[17] J. M. Burgers, Communicated by letter.
[18] C. Wieselsberger, Physik. Z. **23,** 219 (1922).
[19] H. S. Allen, Phil. Mag. **50,** 323 (1900).
[20] Sir Geoffrey Taylor, Proc. Roy. Soc. London [**A**]**201,** 192 (1950).
[21] D. J. Lewis, Proc. Roy. Soc. London [**A**]**202,** 81 (1950).
[22] W. R. Lane, Ind. Eng. Chem. **43,** 1261 (1951).
[23] W. H. Heybey, Navord Report No. 3594 (December 1953).
[24] A. H. Shapiro, Compressible fluid flow, p. 886 (Ronald Press Co., New York, N. Y., 1954).

WASHINGTON, February 1, 1957.

U. S. GOVERNMENT PRINTING OFFICE: 1958